

Research Articles | Behavioral/Cognitive

Two prediction error systems in the nonlemniscal inferior colliculus: ‘spectral’ and ‘non-spectral’

<https://doi.org/10.1523/JNEUROSCI.1420-23.2024>

Received: 27 July 2023

Revised: 3 April 2024

Accepted: 10 April 2024

Copyright © 2024 the authors

This Early Release article has been peer reviewed and accepted, but has not been through the composition and copyediting processes. The final version may differ slightly in style or formatting and will contain links to any extended data.

Alerts: Sign up at www.jneurosci.org/alerts to receive customized email alerts when the fully formatted version of this article is published.

Two prediction error systems in the nonlemniscal inferior colliculus: ‘spectral’ and ‘non-spectral’

Guillermo V. Carbajal^{1,2}, Lorena Casado-Román^{1,2} & Manuel S. Malmierca^{1,2,3*}

¹ Cognitive and Auditory Neuroscience Laboratory (CANELAB), Institute of Neuroscience of Castilla y León (INCYL), Salamanca, Spain

² Institute for Biomedical Research of Salamanca (IBSAL), Salamanca, Spain

³ Department of Cell Biology and Pathology, Faculty of Medicine, University of Salamanca, Salamanca, Spain

* Corresponding author

ORCID

GVC: <https://orcid.org/0000-0001-5266-1941>

LCR: <https://orcid.org/0000-0002-9583-2402>

MSM: <https://orcid.org/0000-0003-0168-7572>

eMails

MSM: msm@usal.es, phone +34 923 294 500 ext. 5301 or ext. 6571 or ext. 5333

Abbreviated title: Two PE systems in the IC cortices

Keywords: SSA/stimulus-specific adaptation, deviance detection, repetition suppression, predictive processing, subcortical, single units, linear model.

Number of pages: 79

Number of figures (7) and tables (3)

Number of words for abstract (250), introduction (648) and discussion (1500)

Conflict of interest: The authors declare no competing financial interests.

Acknowledgments: This work was supported by the Spanish Ministry of Science and Innovation (MICIN) [grant number PID2019-104570RB-I00]; the Ramón Areces Foundation, Madrid, Spain [grant number CIVP20A6616]; and a MICIN PhD Fellowship held by GVC [grant number BES-2017-080030]. The funders had no role in study design, data collection and analysis, decision to publish, or preparation of the manuscript. We thank Drs Edward L Bartlett and Douglas L Oliver for their insightful comments on preliminary versions of this manuscript. We thank Drs Javier Nieto-Diego, Gloria G Parras, and Catalina Valdés-Baizabal for facilitating data to increase our samples. We also thank Mr Antonio Rivas Cornejo and Ms María Torres Valles for their support with histological procedures.

35 **Abstract**

36 According to the predictive processing framework, perception emerges
37 from the reciprocal exchange of predictions and prediction errors (PE) between
38 hierarchically organized neural circuits. The nonlemniscal division of the inferior
39 colliculus (IC) is the earliest source of auditory PE signals, but their neuronal
40 generators, properties and functional relevance have remained mostly undefined.
41 We recorded single-unit mismatch responses to auditory oddball stimulation at
42 different intensities, together with activity evoked by two sequences of alternating
43 tones to control frequency-specific effects. Our results reveal a differential
44 treatment of the unpredictable 'many-standards' control and the predictable
45 'cascade' control by lemniscal and nonlemniscal IC neurons that is not present in
46 the auditory thalamus or cortex. Furthermore, we found that frequency response
47 areas of nonlemniscal IC neurons reflect their role in subcortical predictive
48 processing, distinguishing 3 hierarchical levels: (1) Nonlemniscal neurons with
49 sharply tuned receptive fields exhibit mild repetition suppression without signaling
50 PEs, thereby constituting the input level of the local predictive processing
51 circuitry. (2) Neurons with broadly tuned receptive fields form the main, 'spectral'
52 PE signaling system, which provides dynamic gain compensation to near-
53 threshold unexpected sounds. This early enhancement of saliency reliant on
54 spectral features was not observed in the auditory thalamus or cortex. (3)
55 Untuned neurons form an accessory, 'non-spectral' PE signaling system, which
56 reports all surprising auditory deviances in a robust and consistent manner,
57 resembling nonlemniscal neurons in the auditory cortex. These nonlemniscal IC
58 neurons show unstructured and unstable receptive fields that could result from

59 inhibitory input controlled by corticofugal projections conveying top-down
60 predictions.

61

62 **Significant Statement**

63 Frequency response areas of nonlemniscal neurons in the inferior
64 colliculus correlate with certain predictive processing traits, distinguishing two
65 prediction error systems. The 'spectral' system comprises neurons with broadly
66 tuned receptive fields and is exclusively at play in the nonlemniscal inferior
67 colliculus. It generates prediction errors only to low-intensity deviant sounds and
68 is biased towards ascending changes in frequency. Hence, it provides early gain
69 compensation to near-threshold but informative acoustic events, thereby
70 facilitating efficient auditory discrimination under challenging conditions. The
71 'non-spectral' PE system reports on unexpected auditory events, uninfluenced by
72 the acoustic spectral characteristics of deviant sounds. This accessory system
73 comprises untuned neurons with disorganized and dynamic receptive fields,
74 which conceivably receive top-down predictions from higher-order levels of the
75 auditory hierarchy.

76

77 **List of Abbreviations**

- 78 **AC:** auditory cortex.
- 79 **CAS:** cascade control condition.
- 80 **SPL:** sound pressure level.
- 81 **DEV:** deviant condition.
- 82 **FRA:** frequency response area.
- 83 **IC:** inferior colliculus.
- 84 **iMM:** index of neuronal mismatch.
- 85 **iPE:** index of prediction error.
- 86 **iRS:** index of repetition suppression.
- 87 **MGB:** medial geniculate body.
- 88 **MSC:** many standards control condition.
- 89 **PE:** prediction error.
- 90 **STD:** standard condition.
- 91 **U-neurons:** nonlemniscal IC neurons
92 showing U-shaped FRAs.
- 93 **V-neurons:** nonlemniscal IC neurons
94 showing V-shaped FRAs.
- 95 **W-neurons:** nonlemniscal IC neurons
96 showing multi-peaked FRAs.
- 97 **X-neurons:** nonlemniscal IC neurons
98 showing mosaic FRA
- 99

100 **Introduction**

101 Probability-biased processing of auditory input first appears at the inferior
102 colliculus (IC; for review, see Malmierca et al., 2019). During an auditory oddball
103 paradigm (Figure 1A), certain IC neurons reduce discharges to standard (STD)
104 tones while responding vigorously to deviant (DEV) conditions (Malmierca et al.,
105 2009). The resulting neuronal mismatch response has been interpreted as early
106 predictive activity within the auditory pathway (for reviews, see Carbajal and
107 Malmierca, 2018, 2020; Tabas and von Kriegstein, 2021). According to the
108 predictive processing framework (Friston, 2003, 2009, 2010; Hohwy, 2013), high-
109 order neural networks develop predictions to inhibit input from lower levels when
110 it fits into the current predictive model, while lower-order levels signal back
111 prediction errors (PE) whenever expectations are not met. Although hierarchical
112 predictive processing was originally conceived for cortical networks (Rao and
113 Ballard, 1999; Friston, 2005; Friston and Kiebel, 2009a; Bastos et al., 2012; Keller
114 and Mrsic-Flogel, 2018), empirical testing in the auditory system is expanding the
115 framework into subcortical territory, as early as the IC (Parras et al., 2017; Tabas
116 et al., 2020; Valdés-Baizabal et al., 2020; Lesicko et al., 2022; Tabas and von
117 Kriegstein, 2024).

118 The IC constitutes a crucial relay station of the ascending auditory pathway
119 that gives rise to two parallel lines of processing (Cant and Oliver, 2018; Liu et
120 al., 2024). The lemniscal pathway that emerges from the central nucleus presents
121 a sharp tonotopy with minimal cortical input, whereas the nonlemniscal pathway
122 that originates from the IC cortices shows a blurred tonotopy under heavy cortical
123 input (Schreiner and Langner, 1997; Malmierca, 2015). In a previous study

124 (Parras et al., 2017), we performed extracellular recordings in both divisions of
125 the IC (Figure 1C), medial geniculate body (MGB) of the thalamus, and auditory
126 cortex (AC), while controlling frequency-specific adaptation induced during the
127 oddball paradigm (Figure 1A) by means of two control sequences of alternating
128 tones without consequent repetitions: cascade (CAS) and many-standards
129 control (MSC; Figure 1B; Ruhnau et al., 2012). Using control-evoked activity as
130 a benchmark, each neuronal mismatch response was dissociated in two
131 components: (1) repetition suppression (Garrido et al., 2009a; Auzztulewicz and
132 Friston, 2016; Grotheer and Kovács, 2016), indexed as attenuation of the STD-
133 evoked response that could be accounted for by frequency-specific effects (Mill
134 et al., 2011; Taaseh et al., 2011); and (2) PE, indexed as an enhancement of the
135 DEV-evoked response due to predictive processing activity (Figure 1D). This
136 study revealed the IC cortices as the earliest source of auditory PE signals, which
137 amplified as they ascended through the nonlemniscal pathway into the AC in a
138 hierarchical distribution (Parras et al., 2017). Combining this method (Figure 1)
139 with microiontophoresis unveiled that this early flow of PE signals is modulated
140 by dopaminergic input (Valdés-Baizabal et al., 2020). A recent study using
141 optogenetic inactivation of the auditory corticocollicular feedback in awake mice
142 revealed the critical role of top-down input in subcortical PE signaling (Lesicko et
143 al., 2022). Neuroimaging data from humans also reflect predictive activity at
144 midbrain level (Slabu et al., 2012; Cacciaglia et al., 2015; Tabas et al., 2020;
145 Tabas and von Kriegstein, 2024). However, an in-depth analysis of neural
146 generators and functional properties of early auditory PEs is still lacking.

147 The present study aims to characterize the unique traits of PE signaling in
148 the IC, as compared to that in the MGB and AC, by correlating it with sound

149 intensity, direction of frequency changes, and neuronal receptive fields. Our
150 results reveal a dual nature of predictive processing in the IC cortices that is not
151 present in higher regions of the auditory pathway. PE signaling in nonlemniscal
152 IC neurons with broad receptive fields is fundamentally dependent on certain
153 spectral features, whereas untuned neurons with unstructured and dynamic
154 receptive fields disregard acoustic aspects when reporting unexpected input. For
155 descriptive purposes, we will refer to the distinct predictive activity of these two
156 neural populations, respectively, as the 'spectral' and 'non-spectral' PE systems
157 of the IC cortices.

158

159 **Materials and Methods**

160 **Ethics Statement**

161 All surgical procedures were approved by the Bioethics Committee for
162 Animal Care of the University of Salamanca (USAL-ID-195 and USAL-ID-574)
163 and performed in compliance with the standards of the European Convention
164 ETS 123, the European Union Directive 2010/63/EU, and the Spanish Royal
165 Decree 53/2013 for the use of animals in scientific research.

166

167 **Surgical procedures**

168 The surgical and recording procedures were as described elsewhere
169 (Nieto-Diego and Malmierca, 2016; Parras et al., 2017; Valdés-Baizabal et al.,
170 2020). Surgical anesthesia was first induced with (1) a mixture of ketamine

171 (100 mg/Kg) and xylazine (20 mg/Kg) injected intramuscularly and then
172 maintained with urethane (0.8 g/Kg) injected intraperitoneally or (2) directly
173 induced with urethane (1.5 g/kg, intraperitoneally). To ensure a stable deep
174 anesthetic level, supplementary doses of urethane (~0.5 g/Kg) were
175 administered intraperitoneally when the rat recovered pedal withdrawal reflexes.
176 Urethane was chosen over other anesthetic agents because it preserves normal
177 neural activity better, having a modest, balanced effect on inhibitory and
178 excitatory synapses (Maggi and Meli, 1986; Hara and Harris, 2002; Sceniak and
179 MacIver, 2006; Duque et al., 2016).

180 Normal hearing of rats was verified by recording the auditory brainstem
181 responses subcutaneously with needle electrodes. An RZ6 Multi I/O Processor
182 (Tucker-Davis Technologies) was used to acquire the auditory brainstem
183 response, which was processed with BioSig software (Tucker-Davis
184 Technologies) before beginning each experiment. Stimuli used to elicit the
185 auditory brainstem response consisted of 0.1 ms clicks at a rate of 21 clicks/s,
186 delivered monaurally to the right ear in 10 dB steps, from 10 to 90 decibels of
187 sound pressure level (dB SPL), in a closed system through a Beyer DT-770
188 earphone (0.1–45 kHz) fitted with a custom-made cone and coupled to a small
189 tube (12 G) sealed in the ear.

190 Once normal hearing had been confirmed, a cannula was installed in the
191 trachea to provide artificial ventilation to the rat with monitored expiratory CO₂,
192 given that urethane depresses respiratory function. Likewise, to maintain body
193 temperature at 37±1 °C, rats were introduced a rectal thermometer and placed
194 on a homeothermic blanket system (Cibertec). The head was stabilized in a

195 stereotaxic frame with a bite bar and 2 hollow specula replacing the ear bars. A
196 sound delivery system was accommodated within the right hollow speculum.
197 Eyes were protected with a drop of ophthalmic gel. To prevent an excess of
198 bronchial secretions, 0.1 mg/Kg of atropine sulfate was administrated
199 subcutaneously. To ameliorate brain edema, 0.25 mg/Kg of dexamethasone was
200 injected intramuscularly. To prevent dehydration, 5 mL of glucosaline solution
201 was administrated subcutaneously. The scalp was shaved, and the revealed skin
202 was disinfected with povidone-iodine. Using a scalpel, an incision was opened
203 along the midline to expose the skull, and the periosteum covering the parietal
204 and the most rostral part of the occipital bones was retracted. Using a dental drill,
205 a round craniotomy was performed in the caudal part left parietal bone, just rostral
206 to the lambdoid suture and lateral to the sagittal suture, thereby exposing the
207 cerebral cortex overlying the left IC. The exposed dura was removed, and the
208 tissue beneath it was covered with 2% agar to prevent desiccation during the
209 recording session.

210

211 **Data acquisition procedures**

212 The dataset used in this study is a compilation of extracellular single-unit
213 recordings performed throughout a period of 7 years following the same
214 experimental design (Figure 1). Most of the neurons from the MGB and the AC
215 have featured in previous studies (Parras et al., 2017, 2021; Pérez-González et
216 al., 2021). In the present study, they are combined and reanalyzed for the
217 purpose of comparing their population trends with those of the IC, which is the
218 focus of the present study. Regarding the IC, 125 neurons in the current dataset

219 have featured in two preceding studies (Parras et al., 2017; Valdés-Baizabal et
220 al., 2020), while the remaining 190 units of the sample (60 %) were specifically
221 recorded for this purpose. We will describe the acquisition procedures for these
222 IC data in the following, while the methods followed for the MGB and AC data are
223 detailed elsewhere (Parras et al., 2017).

224 Tungsten microelectrodes used to record the extracellular activity of IC
225 neurons were crafted with a tip impedance of 1.5–3.5 M Ω at 1 kHz following the
226 ensuing protocol (Merrill and Ainsworth, 1972). Experiments were performed
227 inside a sound-insulated and electrically shielded chamber. The microelectrode
228 was mounted on a holder over the exposed cortex, forming an angle of 20°
229 perpendicularly rostral to the coronal plane. Using a piezoelectric
230 micromanipulator (Sensapex), the electrode was inserted into the brain while
231 measuring the penetration depth until strong spiking activity synchronized with
232 the train of searching stimuli could be identified. All sound stimuli were generated
233 using the RZ6 Multi I/O Processor (Tucker-Davis Technologies) and custom
234 software programmed with OpenEx Suite (Tucker-Davis Technologies) and
235 MATLAB (Mathworks). In search of evoked auditory neuronal responses from the
236 IC, white noise bursts and sinusoidal pure tones of 75 ms duration with 5 ms rise-
237 fall ramps were presented, varying stimuli parameters manually to prevent
238 frequency-specific adaptation.

239 Once the activity of a single neuron was clearly isolated, only pure tones
240 were used to record the experimental stimulation protocols, which ran at 4 stimuli
241 per second. Stimuli were delivered monaurally to the ear contralateral to the left
242 IC through a close-field speaker. We calibrated the speaker using a ¼-inch

243 condenser microphone (model 4136, Brüel&Kjær) and a dynamic signal analyzer
244 (Photon+, Brüel&Kjær) to ensure a flat spectrum up to 76 ± 3 dB SPL between
245 0.5 and 45 kHz, and that the second and third signal harmonics were at least 40
246 dB lower than the fundamental at the loudest output level.

247 Analog signals were digitized with a RZ6 Multi I/O Processor, a RA16PA
248 Medusa Preamplifier, and a ZC16 headstage (Tucker-Davis Technologies) at 12
249 kHz sampling rate and amplified 251x. Neurophysiological signals of spiking
250 activity were band-pass filtered between 0.5 and 3 kHz using a second-order
251 Butterworth filter. Stimulus generation, neuronal response processing, and
252 visualization were controlled online with custom software created with the
253 OpenEx suite (Tucker-Davis Technologies) and MATLAB. A unilateral threshold
254 for automatic action potential detection was manually set at about 2–3 standard
255 deviations of the background noise. Spike waveforms were displayed on the
256 screen and overlapped on each other in a pile plot to facilitate isolation of single
257 unit activity. The recorded action potentials were considered to belong to a single
258 unit only when all spike waveforms were akin, clearly separable from other
259 smaller units and the background noise, and the spike-amplitude-to-noise-ratio
260 of the average waveform was larger than 5.

261
$$\text{Signal/Noise Ratio} = \frac{\max(\bar{x}(\text{waveforms})) - \min(\bar{x}(\text{waveforms}))}{\text{Std}(\text{waveforms})}$$

262

263 **Experimental design**

264 A map of response magnitude for each frequency-intensity combination
265 was first computed, representing the receptive field of the single unit in a

266 frequency response area (FRA; Figures 4A and 5A). The stimulation protocol to
267 obtain the FRA consisted of a sequence of sinusoidal pure tones ranging between
268 0.7–44 kHz, 75 ms of duration with 5 ms rise-fall ramps, presented at a 4 Hz rate,
269 randomly varying frequency and intensity (3–5 repetitions of all tones).

270 Then, 10 frequencies separated by 0.5 octave steps at a fixed sound
271 intensity (usually 10–20 dB above minimal response threshold) were selected so
272 that at least 2 consecutive tones fell within the excitatory region of the FRA. These
273 10 tones were used to generate the control sequences (Figure 1B), and adjacent
274 pairs within the excitatory region of the FRA were used to create oddball
275 sequences (Figure 1A). All sequences were 400 tones in length, presented at a
276 constant rate of 4 Hz and at a constant intensity between 10 and 70 dB SPL, in
277 steps of 10 dB SPL.

278 A first complete experimental set, comprised of oddball and control
279 sequences in both their ‘ascending’ and ‘descending’ versions (Figure 1A and B),
280 was presented at a chosen intensity. Whenever it was possible to maintain a
281 certain neuron isolated over a long period of time, another set would be presented
282 at a different intensity. Usually, one intensity would be <40 dB SPL (low) and the
283 other >40 dB SPL (high), but this depended on the receptive field of each neuron
284 as shown by the FRA. The presentation of a set at different intensity levels did
285 not follow any particular order. Sometimes the stability of the signal allowed to
286 record multiple complete sets of sequences at several levels of intensity.
287 However, such occurrence was relatively rare, since our recording protocol did
288 not permit re-isolation attempts. When signal quality dropped below standards,
289 the recording was interrupted, and the incomplete set discarded.

290 A 10% probability was used to pseudo-randomly distribute tones across
291 control sequences within chunks of 10 stimuli, as well as to scatter DEV tones
292 across the oddball sequence. Since only the last STD tones before a DEV were
293 considered for analysis, this method resulted in 40 trials of DEV, STD, MSC and
294 CAS for each given tone of interest. In the oddball paradigm, the first 10 tones
295 were always STD, and a minimum of 3 STD preceded each DEV, which were
296 pseudo-randomly presented with a 10% probability. Oddball sequences were
297 labeled either 'ascending' or 'descending', depending on whether DEV had a
298 higher or lower frequency than STD, respectively (Figure 1A). DEV and STD
299 conditions of the oddball paradigm will be used to obtain neuronal mismatch
300 measurements.

301 One limitation of the neuronal mismatch measurements obtained using the
302 oddball paradigm is that the activity related to high-order processes of PE
303 signaling cannot be distinguished from lower-order effects such as frequency-
304 specific adaptation (Todorovic and de Lange, 2012; Carbajal and Malmierca,
305 2018). The controls allow assessing the relative contribution of both higher- and
306 lower-order processes to the overall mismatch response (Ruhnau et al., 2012).
307 These controls of the auditory oddball paradigm are tone sequences that must
308 meet 3 criteria: (1) to feature the same tone of interest with the same presentation
309 probability as that of the DEV (i.e., 10%); (2) to induce an equivalent state of
310 refractoriness by presenting the same rate of stimulus per second (i.e., 4 Hz);
311 and (3) to present no recurrent repetition of any individual stimulus, especially the
312 tone of interest (Carbajal and Malmierca, 2020).

313 These 3 presentation criteria prevent the short-term dynamics of
314 frequency-specific adaptation in the IC while keeping the long-term dynamics at
315 a minimum (Zhao et al., 2011). Eliminating this minimum would be impractical
316 due to the long-lasting effects of frequency-specific adaptation, which in the rat
317 IC have been reported at presentation rates of up to 1 repetition per second
318 (Pérez-González et al., 2005; Zhao et al., 2011). Consequently, even DEV-
319 evoked responses manifest some marginal frequency-specific adaptation
320 (Malmierca et al., 2009), and will similarly affect tones in a control sequence when
321 presented at equal rate and probability. Note that the objective of these criteria is
322 not to avoid inducing frequency-specific adaptation altogether during the control
323 sequences. Their aim is to guarantee that the response to the tone of interest is
324 subject to similar amounts of refractoriness and adaptation in DEV and control
325 conditions, thereby allowing comparisons to reveal the influence of higher-order
326 processes.

327 Hence, we can assess the portion of the mismatch response (DEV–STD)
328 that can be attributed to frequency-specific adaptation induced during the STD
329 train (Ulanovsky et al., 2003; Jääskeläinen et al., 2004; Mill et al., 2011). When
330 the auditory-evoked response is similar or higher during the control than in DEV,
331 then the mismatch response can be fully accounted for by repetition suppression,
332 and no higher-order process of PE signaling can be deduced (i.e., $DEV \leq control$;
333 Figure 1D). Otherwise, a stronger response to DEV than to the control unveils a
334 component of the mismatch response that can be better explained by PE
335 signaling (i.e., $DEV > control$; Figure 1D).

336 To dissociate the relative contribution of frequency-specific effects from
337 genuine PE signaling (Figure 1D), we generated 2 different controls for our
338 oddball paradigms: MSC and CAS (Figure 1B). MSC presents the tone of interest
339 embedded in a random sequence of assorted tones, where each tone shares the
340 same 10% presentation probability as DEV in the oddball paradigm (Schröger
341 and Wolff, 1996; Jacobsen et al., 2003). However, some authors have argued
342 that the MSC is not fully comparable with the oddball paradigm, inasmuch as the
343 disorganized succession of tones creates a context of uncertainty that never
344 allows to generate high-precision predictions, whereas STD does (Ruhnau et al.,
345 2012; Harms et al., 2014). Additionally, each tone is preceded by a different tone
346 from trial to trial, which makes it difficult to control any possible effects of spectral
347 processing caused by the differences in frequency steps.

348 CAS tries to overcome the alleged caveats of MSC by presenting tones in
349 a regular fashion, e.g., in an increasing or a decreasing frequency succession or
350 scale. Thus, the stimulus of interest conforms to a regularity—as opposed to
351 DEV—, but not a regularity established by repetition—contrary to STD—, thereby
352 restricting possible frequency-specific effects to a minimum while making CAS a
353 more fitted control than MSC. As an additional advantage, the tone immediately
354 preceding the tone of interest is the same in both oddball and cascade
355 sequences, since only versions following the same direction will be compared
356 (i.e., DEV-ascending versus CAS-ascending, DEV-descending versus CAS-
357 descending). This allows to control for possible spectral sensitivity effects, which
358 are responses to a rise or fall in frequency between 2 successive tones. For these
359 reasons, CAS is usually regarded as a better control for the oddball paradigm
360 (Ruhnau et al., 2012; Harms et al., 2014).

361

362 **Histology and neuroanatomical location**

363 At the end of each experiment, electrolytic lesions were inflicted by
364 applying an electric current of 5 μ A during 5 s through the recording electrode
365 along the recorded tract. If still alive, animals were sacrificed by injecting a lethal
366 dose of pentobarbital, after which they were decapitated. Brains were
367 immediately immersed in a mixture of 4% formaldehyde in 0.1 M PB. After
368 fixation, the neural tissue was cryoprotected in 30% sucrose and sectioned in the
369 coronal plane at 40 μ m thickness on a freezing microtome. Slices were stained
370 with 0.1% cresyl violet to facilitate identification of cytoarchitectural boundaries.
371 Finally, the recorded neurons were assigned to one of the main subdivisions of
372 the IC using the standard sections from a rat brain atlas as reference (Paxinos
373 and Watson, 2007).

374 The main dataset is comprised of 315 auditory neurons recorded in the IC
375 of 51 anesthetized Long Evans rats. Additionally, 161 neurons from the MGB of
376 34 rats, and 181 neurons from the AC of 51 rats from our lab's database were
377 included in this study for comparative purposes. Histological examination of the
378 IC samples revealed that 70 neurons came from the central nucleus of the IC,
379 the lemniscal division. The other 245 collicular neurons were in the cortical
380 regions of the IC, the nonlemniscal division. MGB samples were comprised of 58
381 lemniscal (ventral division) and 103 nonlemniscal neurons (dorsal and medial
382 divisions). The AC sample included 119 neurons from the lemniscal core
383 (primary, anterior, and ventral fields) and 62 neurons from the nonlemniscal belt
384 (posterior and suprarhinal fields).

385

386

387 **Data analysis and visualization**

388 All data analyses and data visualization were performed with MATLAB
389 software, using the built-in functions, the Statistics and Machine Learning toolbox,
390 and custom scripts and functions developed in our laboratory.

391

392

393 *Code accessibility*

394 All data and codes used in this study are available upon direct request to
395 the corresponding author.

396

397 *Baseline-corrected spike counts*

398 Taking the 40 trials available for each tone (kHz) within each condition
399 (DEV, STD, MSC and CAS), a peristimulus time histogram was computed to
400 represent the action potential density over time in spikes per second from -75 to
401 250 ms around stimulus onset. This histogram was smoothed with a 6 ms
402 Gaussian kernel (*ksdensity* function in MATLAB) in 1 ms steps to estimate the
403 spike-density function over time. The baseline spontaneous firing rate was
404 determined as the average firing rate (in spikes/s) during the 75 ms preceding
405 stimulus onset. The excitatory response was measured as the area below the
406 spike-density function and above the baseline spontaneous firing rate, between
407 0 and 180 ms after stimulus onset. In other words, the average level of
408 spontaneous firing within the -75–0 ms time window was subtracted from the

409 activity recorded within the 0–180 ms time window, thereby obtaining a
410 measurement of the evoked firing activity that is referred to as the *baseline-*
411 *corrected spike count*.

412 After subtracting the spontaneous activity, we used a Monte Carlo method
413 to find statistically significant responses evoked by sound within the resulting
414 baseline-corrected spike counts. This approach consists of a probability
415 simulation that withdraws numerical values from several random samplings. First,
416 1000 peristimulus time histograms were simulated using a Poisson model with a
417 constant firing rate equal to the baseline spontaneous firing rate. With this
418 collection of histograms, we generated a null distribution of baseline-corrected
419 spike counts. Finally, we computed the p value of the original baseline-corrected
420 spike count as $p = (g + 1)/(N + 1)$, where g is the count of null measures greater
421 than or equal to the baseline-corrected spike count and $N = 1000$ is the size of
422 the null sample. Hence, the Monte Carlo method allowed us to remove any unit-
423 frequency combinations without significant firing activity evoked in response to at
424 least one of the conditions in each experimental set (DEV, STD, or control).

425

426 *Calculation of predictive processing indices*

427 CAS and MSC were introduced to control for the repetition effects of the
428 oddball paradigm, allowing a dissociation of frequency-specific adaptation into
429 *PE* and repetition suppression components. To adequately compare between
430 responses from different neurons, the spike count evoked by each tone in DEV,
431 STD, and control was normalized as follows:

432
$$DEV_N = \frac{DEV}{N} ; STD_N = \frac{STD}{N} ; control_N = \frac{control}{N}$$

433 Where,

434
$$N = \sqrt{DEV^2 + STD^2 + control^2}$$

435 From these normalized responses, we computed the indices of *neuronal*
436 *mismatch* (iMM), *repetition suppression* (iRS), and *prediction error* (iPE) as:

437
$$iMM = DEV_N - STD_N$$

438
$$iRS = control_N - STD_N$$

439
$$iPE = DEV_N - control_N$$

440 These indices range between -1 and 1. The iMM is largely equivalent to
441 the classic Common Stimulus-Specific Adaptation Index (Ulanovsky et al., 2003;
442 see Supplementary Figure 2 in Parras et al., 2017).

443 Lastly, to analyze the emergence of predictive signals around stimulus
444 presentation, we also calculated the average iPE in 8 time windows of 20 ms
445 width from -50 to 190 ms relative to stimulus onset.

446

447 *FRA analysis and classification*

448 We investigated whether PE signaling in the IC was influenced by the
449 neuronal tuning bandwidth, considering the different morphologies that the FRA
450 of IC neurons can exhibit (Figures 4A and 5A). First, the characteristic frequency
451 (kHz) within each FRA was identified as the sound frequency that evoked a
452 response with the lowest sound intensity. Then, the bandwidth at 30 dB SPL

453 above threshold was measured for each unit by calculating the difference
454 between the base 2 logarithms of the upper and lower frequencies of the tuning
455 curve, expressed in kHz. The most used measure to express the sharpness of
456 frequency tuning is the Q factor. Q_n is defined as the characteristic frequency
457 divided by the bandwidth in kHz at 'n' dB above threshold. Thus, the Q_{30} was
458 calculated, and its correlation with the iPE was tested.

459 In addition, each FRA was classified according to its shape. We
460 established 4 categories following criteria adapted from Hernández et al., (2005):

461 V-shaped FRAs (V; Figures 4A and 5A, first plot) must show a primary-like
462 receptive field, similar to those observed in the auditory nerve fibers. These FRAs
463 exhibit a very steep high frequency slope and a shallower low frequency slope.
464 The low frequency slope might comprise two segments separated by an elbow.
465 One of the low frequency segments has a steeper slope and extends from the tip
466 of the FRA to about 35 dB or more above threshold. The second segment has a
467 very shallow slope, forming the so-called low frequency tail, but it is not always
468 present. For concision, in the text we will refer to nonlemniscal IC neurons
469 showing V-shaped FRAs simply as 'V-neurons' or sharply tuned neurons.

470 Multi-peaked FRAs (W; Figures 4A and 5A, second plot) had two or more
471 excitatory regions separated by an area of little or no response. These FRAs had
472 to meet 3 criteria: (1) the thresholds of at least two of the peaks had to differ by \leq
473 30 dB; (2) separation between peaks had to be maintained for levels \geq 20 dB
474 above minimum thresholds; and (3), firing rate in the peaks had to be of at least
475 \geq 1 spike per trial. For concision, in the text we will refer to nonlemniscal IC
476 neurons showing multi-peaked FRAs simply as 'W-neurons'.

477 U-shaped FRAs (U; Figures 4A and 5A, third plot) responded similarly to
478 a wide range of frequencies at its threshold level and presented relatively shallow
479 slopes on the sides. For concision, in the text we will refer to nonlemniscal IC
480 neurons showing U-shaped FRAs simply as 'U-neurons'. W-neurons and U-
481 neurons may also be collectively referred to as broadly tuned neurons.

482 Mosaic FRAs (X; Figures 4A and 5A, fourth plot) comprised several islands
483 of response and/or inhibition, without revealing any consistent characteristic
484 frequency or clear tuning. These islands of response did not form any particular
485 or stable shape, showing dynamic changes between different mappings of the
486 FRA. For concision, in the text we will refer to nonlemniscal IC neurons showing
487 mosaic FRAs simply as 'X-neurons' or untuned neurons.

488 Our sample did not include some non-V-shaped FRA types featured in
489 other IC studies, such as narrow, closed, high-tilt, and low-tilt FRAs (Hernández
490 et al., 2005; Palmer et al., 2013). This could be due to an experimental bias
491 introduced while choosing adequate neurons to record responses to our
492 stimulation protocol. Narrow, closed, high-tilt, and low-tilt FRAs reflect rather
493 small receptive fields, with little responsive space to place stimuli to generate
494 oddball paradigms and control sequences. Hence, neurons with small receptive
495 fields were most likely deemed unfit for recording the stimulation protocol by the
496 experimenters.

497

498

500 Statistical analyses were carried out using distribution-free, nonparametric
501 tests. These included the Friedman test for baseline-corrected spike counts and
502 normalized responses to DEV, STD, and each control condition (CAS or MSC),
503 as well as for the IMM, iRS, and iPE. For multiple comparison tests, p values were
504 corrected for false discovery rate (FDR = 0.05) using the Benjamini-Hochberg
505 method. A two-way analysis of variance (ANOVA) with Bonferroni-correction for
506 multiple comparisons for factors *processing region* and *control type* was
507 performed to directly compare between normalized responses evoked by the
508 control sequences (CAS and MSC) within each lemniscal and nonlemniscal
509 divisions of the IC, MGB, and AC.

510 To study the influence of the previous tone on the evoked responses of IC
511 neurons during the control sequences (CAS and MSC), each trial on each
512 sequence was extracted. For each individual trial (n), the frequency step in
513 octaves was computed as the absolute value of the tone frequency of the trial (n)
514 minus the tone frequency of the preceding trial ($n-1$), resulting in a 'frequency
515 step' value in octaves. This frequency step could be 0.5 or 4.5 octaves during
516 CAS, where tones are ordered regularly in increasing or decreasing frequency
517 (Figure 2A). In the MSC, tone presentation is pseudorandom, so the frequency
518 steps between them could be 0.5, 1.0, 1.5, 2.0, 2.5, 3.0, 3.5, 4.0 or 4.5 octaves
519 (Figure 2A). Pairs of MSC and CAS sequences using the same 10 tones
520 presented at the same intensity to the same neuron were normalized by the
521 largest response in either sequence. Then, trials were grouped by frequency step,
522 control type (MSC or CAS) and either recording site (lemniscal or nonlemniscal
523 divisions of IC, MGB or AC) or FRA category (V, W, U or X; only for nonlemniscal

524 IC neurons), and the normalized average response was computed for each
525 group. A two-way ANOVA with Scheffé's procedure correction for multiple
526 comparisons with *control type* (MSC or CAS) and *frequency step* (0.5 to 4.5
527 octaves in 0.5-octave steps) as factors was performed separately for each
528 neuronal group. ANOVA results that are especially relevant to this study are at
529 display in the comparison matrices (Figures 2 and 7), where the tone of green
530 codifies significance level. Wherever average normalized responses were
531 significantly different between two groups, the magnitude of such difference is
532 expressed as a percentage.

533 Ten linear models were fitted using the *fitlm* function in MATLAB, with
534 robust options. First, we replicated the 'global model' of Parras et al. (2017)
535 regarding the hierarchical distribution of iPE (dependent variable) along the
536 auditory pathway by introducing *region* (IC, MGB, or AC) and *pathway* (lemniscal
537 or nonlemniscal) as predictor variables. The reference levels chosen for these
538 factors were 'lemniscal' and 'IC', as no traces of PE signals have been observed
539 in the central nucleus of the IC (Parras et al., 2017). Second, we expanded the
540 original global model to account for spectral properties of the stimulation by
541 incorporating 2 more predictors: sound *intensity* (1 to 7 B SPL in 1 B SPL steps;
542 1 B SPL = 0.1 dB SPL) and DEV *direction* (ascending or descending). Third, a
543 post-hoc 'local model' using these 2 predictors (sound *intensity* and DEV
544 *direction*) was fitted for each auditory region that yielded significant iPE values
545 (nonlemniscal IC, nonlemniscal MGB, lemniscal AC and nonlemniscal AC), as
546 well as for each FRA-type group of nonlemniscal IC neurons (V-shaped,
547 multipeaked, U-shaped, and mosaic). These linear models used the values of 1
548 B SPL and 'descending' as reference to calculate the intercept. Finally, an

549 ANOVA was performed to identify which predictors and interactions between
550 them were significant in each of the resulting linear models: 1 global model
551 (replicating Parras et al., 2017), 1 expanded global model, 4 regional models and
552 4 FRA models.

553

554 **Results**

555 In the following sections, we first describe how tonal succession in CAS
556 and MSC is encoded by means of spectral processing in the lemniscal IC and
557 predictive processing in the nonlemniscal IC. Second, we present an updated
558 global model of the auditory pathway that confirms the hierarchical distribution of
559 the index of prediction error (iPE) from the nonlemniscal IC to the AC, replicating
560 Parras et al. (2017) with much larger sample sizes (IC: 82→315 units, 384%
561 increase; MGB: 58→161 units, 278% increase; AC: 70→181 units, 259%
562 increase), as well as expanding the linear model from 2 to 4 predictor variables:
563 region, pathway, intensity and DEV direction. Third, we introduce new local iPE
564 models for the nonlemniscal IC, nonlemniscal MGB, and both lemniscal and
565 nonlemniscal AC, which revealed the unique sensitivity of PE signaling in the
566 nonlemniscal IC to sound intensity and direction of frequency change. Finally, we
567 demonstrate the dependency between iPE values and the shape of the receptive
568 field or FRA in IC neurons, which defined the ‘spectral’ and ‘non-spectral’ PE
569 systems in the nonlemniscal IC.

570

571 **Differential processing of MSC and CAS in each IC division**

572 In agreement with previous observations in rodents (Parras et al., 2017,
573 2021; Casado-Román et al., 2020; Valdés-Baizabal et al., 2020; Lesicko et al.,
574 2022) and humans (Wiens et al., 2019), the global responses elicited by CAS and
575 MSC did not differ significantly within each of the hierarchical levels studied: IC,
576 MGB, and AC (two-way ANOVA with Bonferroni-correction for multiple
577 comparisons for factors *region* [$F = 250.17, p < 0.001$], *control* [$F = 0.5, p = 0.482$]
578 and their interaction [$F = 0.99, p = 0.424$]). Consequently, calculations using
579 either CAS (Table 1) or MSC (Table 2) yielded equivalent results. Hence, the
580 models presented in the following sections use the results obtained with CAS,
581 given its methodological advantages (see *Experimental Design in Materials and*
582 *Methods*; Ruhnau et al., 2012; Harms et al., 2014).

583 MSC and CAS present different frequency steps between successive
584 tones (Figure 2A). We analyzed how the previous tone in the control sequence
585 could be influencing the normalized neuronal evoked response in the IC, as well
586 as the MGB and AC (two-way ANOVA with Scheffé's procedure correction for
587 multiple comparisons, using *control type* [MSC or CAS] and *frequency step* [from
588 0.5 to 4.5 octaves in 0.5-octave steps] as factors). In the following, we provide a
589 detailed account of results regarding the IC, whereas MGB and AC results will be
590 just succinctly outlined for comparative purposes.

591 Regarding the IC, the *frequency step* (lemniscal IC: $F = 307.56, p < 0.001$;
592 nonlemniscal IC: $F = 107.15, p < 0.001$), and the *interaction* between control type
593 and frequency step (lemniscal IC: $F = 28.51, p < 0.001$, nonlemniscal IC: $F =$

594 107.15, $p < 0.001$) had an influence on the evoked response, but not the *control*
595 *type* alone.

596 In the lemniscal IC, frequency change from the preceding tone exerted
597 noticeable influence, since a sizable proportion of responses to various octave
598 separations were statistically different from each other (Figure 2B). Lemniscal IC
599 neurons distinguished ten frequency steps more than their nonlemniscal
600 counterparts, implying finer spectral resolution. Furthermore, equal frequency
601 step comparisons across control sequences (0.5- and 4.5-octave steps; Figure
602 2A, in green) revealed that lemniscal IC neurons responded similarly to equal
603 frequency changes presented within CAS and MSC (Figure 2B, black dotted
604 circles).

605 On the other hand, contrast between frequency steps had to be larger in
606 the nonlemniscal IC to observe a significant difference in spike counts (Figure
607 2C, in green), indicating more limited spectral resolution. However, nonlemniscal
608 IC neurons responded differently to equal frequency steps depending on where
609 they were presented, within CAS or within MSC (Figure 2C, white circles), in line
610 with the tenets of the predictive processing framework. The 0.5-octave step
611 yielded larger spike counts when presented in MSC than in CAS (Figure 2C,
612 upwards black arrow). During the MSC, all frequency changes are unpredictable,
613 including the 0.5- and 4.5-octave steps (Figure 2A, in green). In contrast, 0.5-
614 octave steps are very predictable during the CAS, and thereby susceptible to
615 expectation suppression (Garrido et al., 2009b; Todorovic and de Lange, 2012;
616 Stefanics et al., 2014; Auksztulewicz and Friston, 2016; Carbajal and Malmierca,
617 2018; Emberson et al., 2019). Yet whenever a scale starts over during CAS,
618 instead of the expected 0.5-octave step, it produces a 4.5-octave leap in the

619 opposite direction. Consequently, the first tone of each scale represents a DEV
620 (Tervaniemi et al., 1994). The resulting PE signal could explain why nonlemniscal
621 IC neurons fired more spikes to frequency changes of 4.5 octaves during CAS
622 than during MSC (Figure 2C, leftwards black arrow). Thus, at the expense of finer
623 spectral resolution, nonlemniscal IC neurons obtain early contextual sensitivity
624 that can be accounted for by predictive processing.

625 Regarding the MGB, the *frequency step* (lemniscal MGB: $F = 40.32$, $p <$
626 0.001 ; nonlemniscal MGB: $F = 23.97$, $p < 0.001$), and the *interaction* between
627 control type and frequency step (lemniscal MGB: $F = 11.87$, $p < 0.001$,
628 nonlemniscal MGB: $F = 26.31$, $p < 0.001$) had an influence on the evoked
629 response, but not the *control type* alone. MGB comparison matrices look mostly
630 like that of the nonlemniscal IC, with the critical difference that MGB neurons
631 could not distinguish between equal frequency steps presented in different
632 sequences (similar to Figure 2C, but significance was lost for the circled
633 comparisons pointed by arrows).

634 Regarding the AC, evoked responses of lemniscal AC neurons were
635 influenced by *frequency step* ($F = 28.16$, $p < 0.001$), and the *interaction* between
636 control type and frequency step ($F = 46.72$, $p < 0.001$), but not the *control type*
637 alone. Similar to the MGB, the comparison matrix of the lemniscal AC looked
638 mostly like that of the nonlemniscal IC, with the critical difference that lemniscal
639 AC neurons could not distinguish between equal frequency steps presented in
640 different sequences (similar to Figure 2C, but significance was lost for the circled
641 comparisons pointed by arrows).

642 On the other hand, evoked responses of nonlemniscal AC neurons were
643 influenced only by *frequency step* ($F = 12.72$, $p < 0.001$), but not the *control type*
644 alone nor the *interaction* between control type and frequency step. In contrast
645 with the other regions, nonlemniscal AC neurons could only distinguish between
646 the 0.5-octave step and the 4.5-octave step of the CAS (Figure 7A).

647

648

649 **Distribution of predictive processing indices along the auditory** 650 **pathway**

651 To find traces of predictive processing activity at neuronal level, a within-
652 region multiple comparison Friedman test was performed between DEV, STD,
653 and control responses, such that each pair of conditions within each auditory
654 region was tested for a difference in medians. The corresponding indices of the
655 IC, MGB, and AC, calculated using normalized spike counts evoked by CAS and
656 MSC, are respectively summarized in Tables 1 and 2. These observations were
657 fitted in a linear model with a robust regression for the iPE along the hierarchy, in
658 an effort to replicate previous results with sample sizes tripling those of the
659 original study (Parras et al., 2017). The model used *region* ('IC', 'MGB', 'AC') and
660 *pathway* (Lemniscal 'Lem', Nonlemniscal 'NonLem') as categorical factors,
661 acquiring values 1 when true and 0 when false. The reference levels chosen for
662 these factors were 'Lem' and 'IC', as no traces of PE signals have been observed
663 in the central nucleus of the IC (Parras et al., 2017). The resulting global model
664 was:

670
$$iPE = -0.059 - 0.033 * MGB + 0.249 * AC + 0.092 * NonLem$$

671
$$+ (0.080 * MGB * NonLem + 0.017 * AC * NonLem)$$

665 where the constant term (intercept = -0.059) is the reference iPE value in
666 lemniscal IC. An ANOVA of this model revealed that the evolution of iPE along
667 the hierarchy could be explained by the processing *region* ($F = 128.50$, $p < 0.001$)
668 and the *pathway* ($F = 54.94$, $p < 0.001$), but not the *interaction* between both
669 factors (in parenthesis; *cf.*, Parras et al. 2017).

672 Median DEV responses were stronger than STD responses all over the IC,
673 resulting in a median iMM = 0.16 in the lemniscal IC ($p < 0.001$, Friedman test)
674 and a median iMM = 0.44 in the nonlemniscal IC ($p < 0.001$). In the lemniscal IC,
675 the median normalized spike count in response to both controls was 0.65, slightly
676 stronger than the 0.59 yielded by DEV. Both DEV and control normalized
677 responses surpassed the 0.43 normalized STD spike count. Hence, the resulting
678 median iRS = 0.21 could account for the whole neuronal mismatch signal in the
679 lemniscal IC ($p < 0.001$), even yielding negative iPE values (Tables 1 and 2).
680 Conversely, in the nonlemniscal IC the median normalized DEV spike count of
681 0.66 surpassed the 0.64 registered for CAS, but not the 0.66 yielded by MSC.
682 When calculated with CAS, this resulted in a significant iPE = 0.02 (Table 1),
683 confirming the presence of significant PE signaling activity at sample level within
684 the nonlemniscal IC ($p < 0.001$). However, this was not the case when using MSC
685 (Table 2). In addition, the median normalized STD spike counts in the
686 nonlemniscal IC was half of those observed in the lemniscal IC (Tables 1 and 2).
687 The resulting median iRS = 0.42 was considerably higher among nonlemniscal
688 neurons than in their lemniscal counterparts ($p < 0.001$).

689 Once previous results were replicated (Parras et al., 2017), we tested how
690 spectral features of the stimulation affected the resulting iPE value in the whole
691 auditory pathway. Two new predictor variables were added to the linear model:
692 sound *intensity* and DEV *direction*. Sound *intensity* was measured in Bels (1 to 7
693 B SPL in 1 B SPL steps). DEV *direction* is a dichotomic variable, so the factor
694 *ascending* acquired the numeric value of 1 when true or 0 when false, while the
695 factor *descending* was used as reference to calculate the intercept. Hence, this
696 expanded model used four predictors: *region* ('IC', 'MGB' or 'AC') and *pathway*
697 (Lemniscal 'Lem' or Nonlemniscal 'NonLem'), sound *intensity* ('SPL', in Bels) and
698 DEV *direction* (ascending 'asc' or descending 'dsc'). The reference levels chosen
699 for these factors were 'IC', 'Lem', 1 B SPL and 'dsc'. The resulting expanded
700 global model was:

$$\begin{aligned}
701 \quad iPE = & 0.008 - 0.293 * MGB - 0.049 * AC + 0.224 * NonLem - 0.015 \\
702 & * SPL + 0.055 * MGB * SPL + 0.067 * AC * SPL - 0.032 \\
703 & * NonLem * SPL + 0.331 * MGB * asc + 0.233 * AC * asc \\
704 & + (0.027 * asc + 0.252 * MGB * NonLem + 0.081 * AC * NonLem \\
705 & + 0.019 * NonLem * asc - 0.004 * asc * SPL - 0.538 * MGB \\
706 & * NonLem * asc - 0.051 * AC * NonLem * asc - 0.022 * MGB \\
707 & * NonLem * SPL - 0.010 * AC * NonLem * SPL - 0.070 * MGB \\
708 & * asc * SPL - 0.054 * AC * asc * SPL + 0.005 * NonLem * asc \\
709 & * SPL + 0.085 * MGB * NonLem * asc * SPL + 0.002 * AC \\
710 & * NonLem * asc * SPL)
\end{aligned}$$

711 An ANOVA revealed that iPE values throughout the auditory pathway
712 could be explained by the processing *region* ($F = 134.90$, $p < 0.001$), *pathway*

713 (F = 54.19, $p < 0.001$), sound *intensity* (F = 37.08, $p < 0.001$), as well as the
714 interaction between *region and intensity* (F = 5.81, $p = 0.003$), *pathway and*
715 *intensity* (F = 9.10, $p = 0.003$), and *region and direction* (F = 3.60, $p = 0.028$).
716 Neither DEV *direction* alone nor the rest of interactions between factors yielded
717 significant effects (between parenthesis). Therefore, the expanded global model
718 reflects the effect of spectral characteristics on auditory predictive processing,
719 especially that of sound intensity. However, the following sections will
720 demonstrate that those spectral influences only affected consistently the PE
721 signaling activity of certain nonlemniscal IC neurons.

722

723 **Local models of predictive processing indices for the IC, MGB,** 724 **and AC**

725 To better understand how spectral features influenced PE signals at each
726 level of the auditory hierarchy, we fitted linear models for each index—i.e., iMM,
727 iPE, and iRS—using *intensity* and *direction* of DEV (ascending or descending as
728 categorical factors that acquired values 1 when true and 0 when false) as
729 predictors for each auditory region (separately) where significant traces of
730 predictive activity were found: the nonlemniscal divisions of IC, MGB, and AC, as
731 well as the lemniscal fields of AC. The acoustic characteristics of oddball
732 stimulation only affected indices in the nonlemniscal IC, but not in the rest of the
733 auditory regions (Figure 3A).

734 The linear model for the iMM in the nonlemniscal IC was:

$$735 \quad iMM = 0.698 - 0.065 * SPL + 0.059 * asc - (0.005 * SPL * asc)$$

736 The IMM reflects the oddball intensity (ANOVA, $F = 204.25$, $p < 0.001$) and
737 direction ($F = 4.77$, $p = 0.029$), but not the interaction between these factors (not
738 significant, in parenthesis).

739 The linear model for the iPE in the nonlemniscal IC was:

$$740 \quad iPE = 0.228 - 0.047 * SPL + 0.052 * asc - (0.000 * SPL * asc)$$

741 Similarly, the iPE could be predicted by intensity (ANOVA, $F = 75.16$, $p <$
742 0.001) and direction ($F = 9.52$, $p = 0.002$), but not their interaction (in parenthesis),
743 whose coefficient was virtually zero.

744 In contrast with observations in the nonlemniscal IC, iPE values in the
745 nonlemniscal MGB, lemniscal AC, and nonlemniscal AC could not be accounted
746 for by any linear model reliant on intensity and direction as predictor variables
747 (note their poor fits as opposed to the nonlemniscal IC in Figure 3A). Therefore,
748 PE signaling in the nonlemniscal IC encodes deviant acoustic information,
749 whereas in higher processing levels PE signaling seems to be driven by more
750 abstract information than the intensity or direction of the auditory input.

751 The iRS remained relatively stable across different intensities and pitch
752 changes (Tables 1 and 2), and therefore, it could not be predicted by linear
753 models reliant on intensity and direction as predictors in any auditory region. In
754 contrast, the IMM and iPE observed in nonlemniscal IC neurons were larger when
755 intensities were softer, as well as in ascending oddball paradigms. As stimulation
756 intensity increased, the PE component progressively decreased (Figure 3A, first
757 plot). Also at higher intensities, a shrunk IMM equated to the iRS (Tables 1 and
758 2). Intensity and direction effects disappeared as input ascended the auditory

759 hierarchy, since no linear model of this kind could be fitted in the nonlemniscal
760 MGB or the AC (Figure 3A). Therefore, changes in the IMM of nonlemniscal IC
761 neurons due to intensity and frequency shifts were caused by how those physical
762 characteristics of the stimuli elicit PE signaling in the auditory midbrain.

763 Considering the tendency described by the linear models of the
764 nonlemniscal IC, we examined population indices dividing the samples of each
765 region into '*low intensities*' (< 40 dB SPL) and '*high intensities*' (\geq 40 dB SPL).
766 Once again, the relationship between the intensity of the stimulation and the
767 magnitude of the PE component within the evoked firing response was evident
768 only in the nonlemniscal IC neurons (Figure 3B), further confirming the
769 tendencies described by the linear models. The neuronal mismatch responses in
770 the nonlemniscal IC were significantly larger ($p < 0.001$) at low intensities (iMM =
771 0.56) than at high intensities (iMM = 0.39). As mentioned in the previous section,
772 the PE component of neuronal mismatch responses in the nonlemniscal IC was
773 rather small and only detectable with CAS (iPE = 0.02) when all the intensities
774 were included in the analysis. However, when the analysis only included the
775 nonlemniscal IC neuronal responses to low intensity stimulation, the median
776 normalized DEV spike counts tended to comfortably surpass those elicited by
777 both controls (Figure 3B, first plot, left violin), resulting in $iPE_{CAS} = 0.12$ ($p < 0.001$)
778 and $iPE_{MSC} = 0.09$ ($p = 0.001$). Conversely, at high intensities, this PE component
779 disappears completely (Figure 3B, first plot, right violin). Results of these
780 analyses using CAS and MSC are summarized in Tables 1 and 2, respectively.

781 Hence, direction of frequency and intensity manipulation only affected the
782 PE component of the mismatch response of nonlemniscal IC neurons, without

783 disrupting their levels of repetition suppression. This remarkable and unique
784 population effect imply that the main function of PE signaling activity in the IC
785 cortices is to enhance the early representation of unexpected sounds that meet
786 certain spectral characteristics, e.g., providing dynamic gain compensation to
787 near threshold but informative auditory input. Nevertheless, a closer inspection
788 of different neuronal types proved that this main population effect of ‘spectral’
789 nature was not the only function of PE signaling in the IC cortices, as detailed in
790 the following section.

791

792 **PE signaling characteristics in the nonlemniscal IC depend on** 793 **FRA shape**

794 Nonlemniscal IC neurons with tuned receptive fields (V, W and U shapes),
795 did not exhibit a significant correlation between Q_{30} factors and iPE values.
796 However, more than 20% of nonlemniscal IC neurons in our sample showed an
797 untuned, ‘mosaic’ FRA type where it was not possible to determine any Q factor,
798 due to the lack of a clear and stable characteristic frequency in their receptive
799 fields. The median $iPE_{CAS} = 0.21$ ($p < 0.001$) and $iPE_{MSC} = 0.15$ ($p < 0.001$) in the
800 group of X-neurons were significantly higher ($p < 0.001$) than the median iPE
801 values observed in the rest of nonlemniscal IC neurons, which were not
802 significantly different from 0.

803 Due to this stark contrast between neural populations of the nonlemniscal
804 IC, all previous analyses were repeated for nonlemniscal IC neurons, dividing the
805 sample into 4 FRA categories: *V-shaped* (V), *multipeaked* (W), *U-shaped* (U) and

806 *mosaic* (X). First, we performed a within-category multiple comparison Friedman
807 test between DEV, STD, and control responses, such that each pair of conditions
808 within each FRA category was tested for a difference in medians. Samples within
809 each FRA category were then further divided into 'low intensities' (< 40 dB SPL)
810 and 'high intensities' (\geq 40 dB SPL) for additional comparisons (Figures 4C). The
811 corresponding indices calculated using both controls are summarized in Table 3.
812 The evolution of predictive processing indices values over time was also analyzed
813 for low and high intensities (Figure 5). In every condition, the iRS appears
814 immediately (Figure 5, cyan lines), whereas the iPE takes longer to emerge, if at
815 all (Figure 5, orange lines).

816 Following the general trend in the nonlemniscal IC, all FRA categories
817 showed robust repetition suppression. However, only W- and U- neurons
818 followed the population trend regarding PE signaling, with significant iPE values
819 only at low intensities. Conversely, V-neurons did not reach significant iPE values
820 in any condition, whereas X-neurons yielded robust iPE values at every level of
821 intensity. This was further confirmed by linear models that used intensity and
822 direction of DEV as predictors of iPE values for each FRA category in the
823 nonlemniscal IC, achieving good fits in the 3 tuned groups, i.e., V-, W-, and U-
824 neurons, as opposed to untuned X-neurons (Figure 4B).

825 Finally, we analyzed how the previous tone in the control sequence could
826 be influencing the normalized evoked response in nonlemniscal IC neurons
827 depending on their FRA type (two-way ANOVA with Scheffé's procedure
828 correction for multiple comparisons, using *control type* [MSC or CAS] and
829 *frequency step* [from 0.5 to 4.5 octaves in 0.5-octave steps] as factors). Again,
830 the 3 tuned groups tended to follow the same response trend, which resembled

831 the general trend of the nonlemniscal IC (Figure 2C). Conversely, X-neurons
832 described a completely different pattern (Figure 7B), more akin to that of the
833 nonlemniscal AC neurons (Figure 7A). All these data, in addition to the unstable
834 and unstructured nature of their receptive fields, seem to set aside X-neurons
835 from the rest of nonlemniscal IC neurons (Figure 6), suggesting higher-order
836 capabilities. In the following, detailed results are provided for each FRA category.

837

838 *Sharply tuned receptive fields: V-neurons*

839 The linear model for V-neurons (Figure 4B, first plot) was:

$$840 \quad iPE_V = 0.067 - 0.024 * SPL + 0.073 * asc + (0.005 * SPL * asc)$$

841 The ANOVA of this model revealed a significant effect of intensity
842 ($F = 5.36$, $p = 0.021$) and direction ($F = 10.75$, $p = 0.001$), but no significant
843 interaction between factors (in parenthesis). Despite model fitness, positive iPE
844 magnitudes in V-neurons were not significant for any sample of evoked firing
845 responses (Table 3; Figures 4 and 5, first column; Figure 6).

846 Regarding frequency step discrimination, V-neuron followed the general
847 tendency of the nonlemniscal IC population, showing evoked responses
848 influenced by *frequency step* ($F = 103.72$, $p < 0.001$), and the *interaction* between
849 control type and frequency step ($F = 86.76$, $p < 0.001$). Comparison matrix of V-
850 neurons was like Figure 2C with exception of the comparison between 0.5-octave
851 steps in MSC and CAS, which significance was lost.

852 Hence, V-neurons lack the high spectral resolution of their lemniscal
853 homologues, but in exchange they manifest some contextual sensitivity. V-

854 neurons do not contribute to the main PE signaling effect observed at population
855 level in the IC cortices, while being subject to stronger repetition suppression than
856 lemniscal IC neurons (Tables 1-3). Therefore, their properties seem somewhat
857 transitional, which hints at the possibility of V-neurons constituting the ‘input level’
858 of the predictive processing circuitry of the IC cortices (Figure 7D).

859

860 *Broadly tuned receptive fields: W- and U-neurons*

861 The linear model for W-neurons (Figure 4B, second plot) was:

$$862 \quad iPE_W = 0.273 - 0.061 * SPL + (0.016 * asc * 0.004 * SPL * asc)$$

863 The iPE_W was predicted only by the intensity of the oddball stimulation
864 (ANOVA, $F = 37.68$, $p < 0.001$), but not for direction or the interaction between
865 factors (both in parenthesis).

866 The linear model for U-neurons (Figure 4B, third plot) was:

$$867 \quad iPE_U = 0.204 - 0.050 * SPL + (0.127 * asc - 0.018 * SPL * asc)$$

868 The iPE_U revealed a significant effect of intensity (ANOVA, $F = 39.70$, $p <$
869 0.001), but not for direction or the interaction between factors (both between
870 parenthesis).

871 In W- and U-neurons, the effect of intensity over the magnitude of the PE
872 component within the neuronal mismatch response became evident when
873 comparing the distribution of normalized DEV- and control-evoked spike counts
874 (Figure 4C, second and third plots), when observing the evolution of the iPE over
875 time (Figure 5, second and third plots), as well as when comparing the median

876 indices of each category at low and high intensity stimulation using both CAS and
877 MSC (Figure 6, Table 3). Traces of PE signaling could be found at low intensity
878 stimulation in W-neurons, but only when using CAS (iPE = 0.11; $p < 0.001$; Figure
879 5B, second plot). For U-neurons, a significant PE component was revealed for
880 low intensity stimulation using both CAS and MSC (iPE = 0.11, $p = 0.003$; Figure
881 5B, third plot).

882 Regarding frequency step discrimination, U-neurons followed the general
883 tendency of the nonlemniscal IC population (at display in Figure 3A), showing
884 evoked responses influenced by *frequency step* ($F = 153.19$, $p < 0.001$), and the
885 *interaction* between control type and frequency step ($F = 88.03$, $p < 0.001$).
886 Comparison matrix of U-neurons was like Figure 2C with exception of the
887 comparison between 0.5-octave steps in MSC and CAS, which significance was
888 lost. In contrast, evoked responses of W-neurons were only influenced by
889 *frequency step* ($F = 26.38$, $p < 0.001$). The comparison matrix reveals that W-
890 neurons could only distinguish between pronouncedly different frequency steps,
891 i.e., the 4.5-octave leap in CAS against frequency steps of 2.5 octaves or smaller.

892 Hence, W- and U-neurons tend to follow the general trends of the
893 nonlemniscal IC population, with rather limited frequency-step discrimination and
894 PE signaling heavily influenced by spectral features of auditory input. In fact, as
895 detailed in the next section, only W- and U-neurons are responsible for the main
896 population effect observed in the IC cortices, revealing them as the true neural
897 substrate of a 'spectral' PE system (Figure 7D).

898

900 In contrast with tuned FRA categories (V, W and U), the linear model of X-
901 neurons did not achieve a good fit, neither did they show any significant effects
902 of intensity, direction, or their interaction (ANOVA; Figure 4B, fourth plot). The
903 size of the PE component found in X-neurons more than doubled that of the
904 previous categories at low intensities using both CAS and MSC (iPE = 0.23, $p <$
905 0.001; Figure 6). When only neuronal responses to high intensity stimulation were
906 selected, we found that only X-neurons were able to preserve their PE component
907 intact (iPE = 0.22, $p <$ 0.001; Figure 5C), whereas the rest of FRA categories
908 ceased issuing PE signals altogether (Figure 6).

909 Therefore, contrary to the general trend in the nonlemniscal IC, X-neurons
910 yielded significantly positive iPE values across all intensities and regardless of
911 DEV direction, more in the vein of the AC (compare fourth column of Figure 4
912 with the third and fourth columns of Figure 3). This differential behavior can be
913 appreciated when comparing the distribution of normalized DEV- and control-
914 evoked spike counts (Figure 4C), when observing the evolution of the iPE over
915 time (Figure 5), as well as when comparing the median indices of each category
916 at low and high intensity stimulation using both CAS and MSC (Figure 6, Table
917 3). This means that X-neurons do not contribute to the main effect of PE signaling
918 observed in the nonlemniscal IC, and thereby are not part of the 'spectral' PE
919 system.

920 Regarding frequency step discrimination, only the *interaction* between
921 control type and frequency step had an influence on the evoked response of X-
922 neurons ($F = 23.52$, $p <$ 0.001). Spectral resolution of X-neurons is the poorest in

923 the IC cortices, only able to contrast between 0.5-octave steps and 4.5-octave
924 leaps in the CAS (Figure 7B), in the same vein of the nonlemniscal AC (Figure
925 7A). This resemblance suggests again a more abstract processing of X-neurons
926 related to higher-order processing regions of the auditory pathway.

927 Hence, in contrast with the main effect observed in nonlemniscal IC
928 processing, X-neurons perform a distinct accessory function that essentially
929 disregard spectral content to consistently report on more contextual information
930 related to novelty or deviances within the auditory scene. X-neurons are thus the
931 neural substrate of a 'non-spectral' PE system (Figure 7D).

932

933 **Discussion**

934 This study reveals the dual nature of predictive processing in the IC
935 cortices, which are endowed with a main, 'spectral' PE system, and an accessory,
936 'non-spectral' PE system. These midbrain-level systems constitute the earliest
937 source of PE signals in the auditory pathway, as confirmed by our expanded
938 linear model for the hierarchical distribution of iPE values. Our results also
939 unravel the differential processing of MSC and CAS by lemniscal and
940 nonlemniscal IC neurons (Figure 2). Most importantly, we expand the established
941 lemniscal-vs-nonlemniscal dichotomy by distinguishing 3 levels of hierarchical
942 processing within the IC cortices (Figures 7D): (1) V-neurons exhibiting mild
943 repetition suppression without signaling PEs constitute the input level of the
944 predictive processing circuitry in the nonlemniscal IC; (2) W- and U-neurons
945 signaling PEs that increase saliency of near-threshold unexpected sounds

946 establish the 'spectral' PE system; and (3) X-neurons consistently reporting all
947 surprising auditory input compose the 'non-spectral' PE system.

948 Sharply tuned receptive fields specialize in lower-order functions such as
949 spectral processing, but are not well suited for complex auditory integration
950 (Oliver et al., 2017). In the IC cortices, however, V-neurons discriminate less
951 frequency steps than their lemniscal homologues while manifesting some
952 contextual sensitivity. Despite not signaling PEs, V-neurons undergo stronger
953 repetition suppression than lemniscal IC neurons, although milder than other
954 nonlemniscal types (Figure 6). These transitional properties arguably make V-
955 neurons the best candidates to funnel 'raw' input from the central nucleus into the
956 predictive processing circuits of the IC cortices. V-shaped receptive fields are
957 inherited from lower auditory nuclei (Le Beau et al., 2001), implying that V-
958 neurons are mainly driven by bottom-up auditory input. Thus, V-neurons may
959 constitute an 'input level' in the nonlemniscal IC, akin to layer IV in the canonical
960 microcircuits of cortical predictive processing (Bastos et al., 2012).

961 Broadly tuned receptive fields can integrate spectral information across
962 many frequency channels (Oliver et al., 2017) and enable the main effect of
963 predictive processing in the IC cortices. W- and U-neurons increase PE signaling
964 to low-intensity sounds and ascending frequency DEVs (Figures 3 and 4).
965 Previously reported changes of neuronal mismatch responses as a function of
966 intensity and frequency in the IC (Duque et al., 2012, 2016) must be due to
967 changes in the PE component, given that repetition suppression tends to remain
968 stable across varying spectral parameters (Figures 5 and 6).

969 Regarding sound intensity, modeling work indicates that neurons are
970 maximally sensitive to change for stimulus ranges where firing rates are below
971 saturation (Abbott et al., 1997), which has been empirically confirmed in the rat
972 IC (Duque et al., 2012). As intensity increases, W- and U-neurons exhaust their
973 discharge capacity to signal PEs. Consequently, iPE decreases with loudness in
974 the IC cortices (Figures 3 to 6), whereas the iRS remains unaffected (Figures 5
975 and 6).

976 Regarding ascending oddballs, enhanced responses compared to
977 descending oddballs have also been reported in electroencephalographic data of
978 rats (Harms et al., 2014) and humans (Peter et al., 2010). This bias might help
979 defining figure-ground relationships in audition (Schneider et al., 2018, 2021).
980 The difficulty of high-pitched sounds to travel long distances means that they
981 usually carry relevant information from our nearby surroundings. Neural
982 representation of surprising changes towards higher frequencies could be
983 facilitated as 'figure' DEV sounds emerging from distant, 'background' STD noise.

984 Hence, W- and U-neurons enhance the saliency of muted unexpected
985 sounds both indirectly, by consistently suppressing repetitive auditory input, and
986 directly, by selectively signaling 'spectral' PEs. This neural substrate constitute
987 the main PE system of the auditory midbrain, which provides gain to subtle but
988 relevant spectral cues, thereby aiding auditory perception under challenging
989 conditions—e.g., when loud background noise masks softer but informative
990 deviant sounds, as described in the visual system (Carandini and Ferster, 1997;
991 Hupé et al., 1998; Michel et al., 2018)—. Most interestingly, only the IC cortices
992 provide this kind of predictive equalization reliant on spectral features (Figure 3),

993 despite MGB and AC neurons presenting multip peaked and U-shaped FRAs
994 (Polley et al., 2007; Parras et al., 2017). Therefore, the 'spectral' PE system
995 cannot be the direct product of the receptive field exclusively, but an emerging
996 property of the nonlemniscal IC circuitry. Furthermore, this agrees with the tenets
997 of predictive processing (Friston and Kiebel, 2009b), as implementing this unique
998 mechanism of dynamic gain in the IC would relieve the MGB and AC from such
999 a loading discrimination task.

1000 Finally, the lack of delimited and stable receptive fields suggests that X-
1001 neurons operate under dynamic inhibitory input (Le Beau et al., 2001) and may
1002 receive corticofugal projections (Lesicko and Geffen, 2022). Perhaps their
1003 receptive field cannot be defined in terms of frequency-intensity combinations
1004 because they are sensitive to more abstract probabilistic structures in auditory
1005 input (Tabas et al., 2020; Peng et al., 2024) or to multisensory input (Aitkin et al.,
1006 1981; Itaya and Van Hoesen, 1982; Tawil et al., 1983; Tokunaga et al., 1984;
1007 Gutfreund et al., 2002; Porter et al., 2007; Gruters and Groh, 2012; Olthof et al.,
1008 2019). Unlike in the rest of nonlemniscal IC neurons, evoked responses in X-
1009 neurons are barely influenced by sound intensity (Figures 4A and 5A). This
1010 prevents discharge saturations caused by loudness, thereby securing enough
1011 dynamic range to always afford increasing firing rates to signal PEs.
1012 Consequently, median iPE values in X-neurons more than double those of the
1013 rest of nonlemniscal IC neurons and are insensitive to intensity variations
1014 (Figures 4 to 6, fourth columns).

1015 Contrasting and complementing the 'spectral' PE system, X-neurons
1016 provide the neural substrate for a 'non-spectral' PE system, which activity bears

1017 more resemblance with that of higher auditory regions. This similarity implies a
1018 functional connection between these neural populations through corticocollicular
1019 projections (Adams, 1980; Herbert et al., 1991; Winer et al., 2002; Malmierca and
1020 Ryugo, 2011; Schofield and Beebe, 2019), which enable an accessory PE system
1021 focused on consistently reporting unexpected auditory events while disregarding
1022 their spectral nature.

1023 In coherence with the canonical microcircuits proposed for cortical
1024 predictive processing (Bastos et al., 2012), deep pyramidal neurons in layers V
1025 and VI generate predictions, which may be imposed on X-neurons through
1026 descending projections (Figure 7C; Games and Winer, 1988). The densest
1027 cortical input that the IC cortices receive comes from nonlemniscal AC fields
1028 (Herbert et al., 1991). Nonlemniscal AC neurons reach the highest iPE values in
1029 the auditory pathway (Parras et al., 2017, 2021) and share remarkable response
1030 similarities with X-neurons (compare fourth columns of Figures 3 and 4, and
1031 Figures 7A and B), further suggesting a functional connection between them.

1032 Although pyramidal projections are glutamatergic (Feliciano and
1033 Potashner, 1995), electrical stimulation of the AC produces excitation and
1034 inhibition in different subpopulations of IC neurons (Mitani et al., 1983; Jen et al.,
1035 1998; Zhou and Jen, 2005; Vila et al., 2019), and AC deactivation yields
1036 disinhibition of some IC neurons (Nwabueze-Ogbo et al., 2003; Popelář et al.,
1037 2016; Blackwell et al., 2020). GABAergic neurons make up to 25% of the rat IC
1038 cortices (Merchán et al., 2005), where distribution of GABA receptors is denser
1039 than in the central nucleus (Milbrandt et al., 1996; Jamal et al., 2012; Choy
1040 Buentello et al., 2015). Moreover, previous studies demonstrated that AC

1041 deactivation reduces neuronal mismatch responses in the IC (Anderson and
1042 Malmierca, 2013) by decreasing the PE component without disrupting repetition
1043 suppression (Lesicko et al., 2022). Hence, deep pyramidal AC neurons could
1044 impose top-down predictions on X-neurons by exciting inhibitory connections
1045 within the IC (Oliver, 2005; Beebe et al., 2016; Ito and Malmierca, 2018; Ito et al.,
1046 2018). As the predictive model receives updates through bottom-up PE signals,
1047 top-down predictions would evolve (Figure 7C), which could explain the unstable
1048 and dynamic nature of mosaic FRAs.

1049 In conclusion, FRA analysis of nonlemniscal IC neurons evidences their
1050 complementary physiological roles and affords the distinction of two early PE
1051 systems. The 'spectral' PE system enhances saliency of near-threshold
1052 surprising sounds, while the 'non-spectral' PE system reports unexpected events
1053 in the auditory scene in a more consistent and abstract manner. Both PE systems
1054 improve overall processing efficiency in the auditory pathway by dynamically
1055 representing informative auditory events already at midbrain level, thereby
1056 sparing MGB and AC resources that can be allocated to processing more
1057 complex aspects of audition. This subcortical capacity to generate early but
1058 contextually rich neural representations of the auditory scene contravenes the
1059 traditional corticocentric understanding (Parvizi, 2009). Hierarchical predictive
1060 processing in the IC cortices may be critical to trigger attention shifts (Jane et al.,
1061 1965; Hu and Dan, 2022), set off rapid eye-head orienting movements toward
1062 sounds (Belenkov and Goreva, 1969; Thompson and Masterton, 1978; Zwiers et
1063 al., 2004; Porter et al., 2007), and assist perception and sound-guided behavior
1064 even before auditory input reaches the cortex (Ryan and Miller, 1977; Brainard
1065 and Knudsen, 1993; Metzger et al., 2006; Rinne et al., 2008; Schelinski et al.,

1066 2022; Escera, 2023; Quass et al., 2023; Lee et al., 2024). Ultimately, our data
1067 supports claims that regard the IC as a functional analog to the primary visual
1068 cortex (Nelken et al., 2003; King and Nelken, 2009), thus furthering the notion of
1069 subcortical cognition (Janacsek et al., 2022).

1070

1071

1072 **CRediT Author Statement**

1073 **GVC:** Conceptualization, Methodology, Software, Validation, Formal Analysis,
1074 Investigation, Data Curation, Writing–original draft, Writing–review and editing,
1075 Visualization.

1076 **LCR:** Software, Validation, Formal Analysis, Investigation, Writing–review and
1077 editing, Visualization.

1078 **MSM:** Conceptualization, Resources, Writing–review and editing, Supervision,
1079 Project Administration, Funding Acquisition.

1080

1081

1082 **REFERENCES**

1083 Abbott LF, Varela JA, Sen K, Nelson SB (1997) Synaptic Depression and
1084 Cortical Gain Control. *Science* (80-) 275:221–224 Available at:
1085 <http://www.sciencemag.org/cgi/doi/10.1126/science.275.5297.221>.

1086 Adams JC (1980) Crossed and descending projections to the inferior colliculus.
1087 *Neurosci Lett* 19:1–5.

1088 Aitkin LM, Kenyon CE, Philpott P (1981) The representation of the auditory and
1089 somatosensory systems in the external nucleus of the cat inferior colliculus.
1090 J Comp Neurol 196:25–40 Available at:
1091 <https://onlinelibrary.wiley.com/doi/full/10.1002/cne.901960104> [Accessed
1092 May 19, 2021].

1093 Anderson LA, Malmierca MS (2013) The effect of auditory cortex deactivation
1094 on stimulus-specific adaptation in the inferior colliculus of the rat. Eur J
1095 Neurosci 37:52–62 Available at: <http://doi.wiley.com/10.1111/ejn.12018>
1096 [Accessed September 12, 2017].

1097 Auksztulewicz R, Friston KJ (2016) Repetition suppression and its contextual
1098 determinants in predictive coding. Cortex 80:125–140.

1099 Bastos AM, Usrey WM, Adams RA, Mangun GR, Fries P, Friston KJ (2012)
1100 Canonical Microcircuits for Predictive Coding. Neuron 76:695–711
1101 Available at: <http://linkinghub.elsevier.com/retrieve/pii/S0896627312009592>
1102 [Accessed February 1, 2018].

1103 Beebe NL, Young JW, Mellott JG, Schofield BR (2016) Extracellular molecular
1104 markers and soma size of inhibitory neurons: Evidence for four subtypes of
1105 GABAergic cells in the inferior colliculus. J Neurosci 36:3988–3999
1106 Available at: <https://www.jneurosci.org/content/36/14/3988> [Accessed
1107 February 17, 2024].

1108 Belenkov NY, Goreva OA (1969) Role of inferior colliculi in orienting reflex.
1109 Neurosci Transl 3:9–16 Available at:
1110 <https://link.springer.com/article/10.1007/BF01124449> [Accessed February
1111 8, 2024].

- 1112 Blackwell JM, Lesicko A, Rao W, De Biasi M, Geffen MN (2020) Auditory cortex
1113 shapes sound responses in the inferior colliculus. *Elife* 9.
- 1114 Brainard MS, Knudsen EI (1993) Experience-dependent plasticity in the inferior
1115 colliculus: A site for visual calibration of the neural representation of
1116 auditory space in the barn owl. *J Neurosci* 13:4589–4608 Available at:
1117 <https://www.jneurosci.org/content/13/11/4589> [Accessed February 8, 2024].
- 1118 Cacciaglia R, Escera C, Slabu L, Grimm S, Sanjuán A, Ventura-Campos N,
1119 Ávila C (2015) Involvement of the human midbrain and thalamus in auditory
1120 deviance detection. *Neuropsychologia* 68:51–58 Available at:
1121 <http://dx.doi.org/10.1016/j.neuropsychologia.2015.01.001>.
- 1122 Cant NB, Oliver DL (2018) Overview of Auditory Projection Pathways and
1123 Intrinsic Microcircuits. In: *The Mammalian Auditory Pathways: Synaptic
1124 Organization and Microcircuits*, pp 7–39. Springer, Cham. Available at:
1125 https://link.springer.com/chapter/10.1007/978-3-319-71798-2_2 [Accessed
1126 February 9, 2024].
- 1127 Carandini M, Ferster D (1997) A tonic hyperpolarization underlying contrast
1128 adaptation in cat visual cortex. *Science* (80-) 276:949–952 Available at:
1129 <http://www.ncbi.nlm.nih.gov/pubmed/9139658> [Accessed June 2, 2018].
- 1130 Carbajal G V., Malmierca MS (2018) The Neuronal Basis of Predictive Coding
1131 Along the Auditory Pathway: From the Subcortical Roots to Cortical
1132 Deviance Detection. *Trends Hear* 22:233121651878482 Available at:
1133 <http://journals.sagepub.com/doi/10.1177/2331216518784822>.
- 1134 Carbajal G V., Malmierca MS (2020) Novelty Processing in the Auditory
1135 System: Detection, Adaptation or Expectation? In: *The Senses: A*

1136 Comprehensive Reference, 2nd ed. (Fritzsche B, Gothe B, eds), pp 749–
1137 776. Elsevier. Available at:
1138 <https://linkinghub.elsevier.com/retrieve/pii/B9780128093245241540>
1139 [Accessed May 20, 2020].

1140 Casado-Román L, Carbajal G V., Pérez-González D, Malmierca MS (2020)
1141 Prediction error signaling explains neuronal mismatch responses in the
1142 medial prefrontal cortex. PLoS Biol 18:e3001019 Available at:
1143 <https://doi.org/10.1371/journal.pbio.3001019> [Accessed April 28, 2021].

1144 Choy Buentello D, Bishop DC, Oliver DL (2015) Differential distribution of GABA
1145 and glycine terminals in the inferior colliculus of rat and mouse. J Comp
1146 Neurol 523:2683–2697 Available at:
1147 <http://doi.wiley.com/10.1002/cne.23810> [Accessed February 4, 2018].

1148 Duque D, Pérez-González D, Ayala YA, Palmer AR, Malmierca MS (2012)
1149 Topographic Distribution, Frequency, and Intensity Dependence of
1150 Stimulus-Specific Adaptation in the Inferior Colliculus of the Rat. J Neurosci
1151 32:17762–17774 Available at:
1152 <http://www.jneurosci.org/content/32/49/17762.long> [Accessed September
1153 12, 2017].

1154 Duque D, Wang X, Nieto-Diego J, Krumbholz K, Malmierca MS (2016) Neurons
1155 in the inferior colliculus of the rat show stimulus-specific adaptation for
1156 frequency, but not for intensity. Sci Rep 6:24114 Available at:
1157 <http://www.ncbi.nlm.nih.gov/pubmed/27066835>
1158 <http://www.pubmedcentral.nih.gov/articlerender.fcgi?artid=PMC4828641>.

1159 Emberson LL, Boldin AM, Robertson CE, Cannon G, Aslin RN (2019)

1160 Expectation affects neural repetition suppression in infancy. *Dev Cogn*
1161 *Neurosci* 37:100597.

1162 Escera C (2023) Contributions of the subcortical auditory system to predictive
1163 coding and the neural encoding of speech. *Curr Opin Behav Sci*
1164 54:101324.

1165 Feliciano M, Potashner SJ (1995) Evidence for a Glutamatergic Pathway from
1166 the Guinea Pig Auditory Cortex to the Inferior Colliculus. *J Neurochem*
1167 65:1348–1357 Available at:
1168 [https://onlinelibrary.wiley.com/doi/full/10.1046/j.1471-](https://onlinelibrary.wiley.com/doi/full/10.1046/j.1471-4159.1995.65031348.x)
1169 [4159.1995.65031348.x](https://onlinelibrary.wiley.com/doi/full/10.1046/j.1471-4159.1995.65031348.x) [Accessed May 22, 2021].

1170 Friston KJ (2003) Learning and inference in the brain. *Neural Networks*
1171 16:1325–1352 Available at:
1172 [https://www.sciencedirect.com/science/article/pii/S0893608003002454?via](https://www.sciencedirect.com/science/article/pii/S0893608003002454?via%3Dihub)
1173 [%3Dihub](https://www.sciencedirect.com/science/article/pii/S0893608003002454?via%3Dihub) [Accessed May 2, 2019].

1174 Friston KJ (2005) A theory of cortical responses. *Philos Trans R Soc B Biol Sci*
1175 360:815–836 Available at:
1176 <http://rstb.royalsocietypublishing.org/cgi/doi/10.1098/rstb.2005.1622>
1177 [Accessed October 1, 2012].

1178 Friston KJ (2009) The free-energy principle: a rough guide to the brain? *Trends*
1179 *Cogn Sci* 13:293–301.

1180 Friston KJ (2010) The free-energy principle: a unified brain theory? *Nat Rev*
1181 *Neurosci* 11:127–138 Available at: <http://www.nature.com/articles/nrn2787>
1182 [Accessed June 4, 2019].

1183 Friston KJ, Kiebel SJ (2009a) Cortical circuits for perceptual inference. *Neural*
1184 *Networks* 22:1093–1104 Available at:
1185 <https://www.sciencedirect.com/science/article/pii/S0893608009001701#b18>
1186 [Accessed December 12, 2018].

1187 Friston KJ, Kiebel SJ (2009b) Predictive coding under the free-energy principle.
1188 *Philos Trans R Soc B Biol Sci* 364:1211–1221 Available at:
1189 <http://www.ncbi.nlm.nih.gov/pubmed/19528002> [Accessed December 13,
1190 2018].

1191 Games KD, Winer JA (1988) Layer V in rat auditory cortex: Projections to the
1192 inferior colliculus and contralateral cortex. *Hear Res* 34:1–25.

1193 Garrido MI, Kilner JM, Kiebel SJ, Stephan KE, Baldeweg T, Friston KJ (2009a)
1194 Repetition suppression and plasticity in the human brain. *Neuroimage*
1195 48:269–279 Available at:
1196 <https://www.sciencedirect.com/science/article/pii/S1053811909006661>
1197 [Accessed February 2, 2018].

1198 Garrido MI, Kilner JM, Stephan KE, Friston KJ (2009b) The mismatch
1199 negativity: a review of underlying mechanisms. *Clin Neurophysiol* 120:453–
1200 463 Available at:
1201 [https://www.sciencedirect.com/science/article/pii/S1388245708012686?via](https://www.sciencedirect.com/science/article/pii/S1388245708012686?via%3Dihub)
1202 [%3Dihub](https://www.sciencedirect.com/science/article/pii/S1388245708012686?via%3Dihub) [Accessed February 4, 2012].

1203 Grotheer M, Kovács G (2016) Can predictive coding explain repetition
1204 suppression? *Cortex* 80:113–124 Available at:
1205 [https://www.sciencedirect.com/science/article/pii/S0010945216000149?via](https://www.sciencedirect.com/science/article/pii/S0010945216000149?via%3Dihub#sec4)
1206 [%3Dihub#sec4](https://www.sciencedirect.com/science/article/pii/S0010945216000149?via%3Dihub#sec4) [Accessed April 27, 2018].

1207 Gruters KG, Groh JM (2012) Sounds and beyond: Multisensory and other non-
1208 auditory signals in the inferior colliculus. *Front Neural Circuits* 6:1–39.

1209 Gutfreund Y, Zheng W, Knudsen EI (2002) Gated visual input to the central
1210 auditory system. *Science* (80-) 297:1556–1559 Available at:
1211 <https://www.science.org/doi/10.1126/science.1073712> [Accessed February
1212 8, 2024].

1213 Hara K, Harris RA (2002) The anesthetic mechanism of urethane: The effects
1214 on neurotransmitter-gated ion channels. *Anesth Analg* 94:313–318
1215 Available at: <http://www.ncbi.nlm.nih.gov/pubmed/11812690> [Accessed
1216 June 3, 2018].

1217 Harms L, Fulham WR, Todd J, Budd TW, Hunter M, Meehan C, Penttonen M,
1218 Schall U, Zavitsanou K, Hodgson DM, Michie PT (2014) Mismatch
1219 negativity (MMN) in freely-moving rats with several experimental controls
1220 Malmierca MS, ed. *PLoS One* 9:e110892 Available at:
1221 <http://dx.plos.org/10.1371/journal.pone.0110892> [Accessed February 2,
1222 2018].

1223 Herbert H, Aschoff A, Ostwald J (1991) Topography of projections from the
1224 auditory cortex to the inferior colliculus in the rat. *J Comp Neurol* 304:103–
1225 122 Available at:
1226 <https://onlinelibrary.wiley.com/doi/full/10.1002/cne.903040108> [Accessed
1227 May 13, 2021].

1228 Hernández O, Espinosa N, Pérez-González D, Malmierca MS (2005) The
1229 inferior colliculus of the rat: A quantitative analysis of monaural frequency
1230 response areas. *Neuroscience* 132:203–217 Available at:

1231 <https://www.sciencedirect.com/science/article/pii/S0306452205000692?via>
1232 [%3Dihub](#) [Accessed February 7, 2018].

1233 Hohwy J (2013) *The predictive mind*. Oxford, England: Oxford University Press.
1234 Available at:
1235 <https://books.google.es/books?hl=en&lr=&id=z7gVDAAAQBAJ&oi=fnd&pg>
1236 [=PP1&dq=info:q91iSdERGM8J:scholar.google.com&ots=DiAM0Xy44s&sig](#)
1237 [=rPAXCTAh2O1u2tLEwWSxb_ScB_Y&redir_esc=y#v=onepage&q&f=false](#)
1238 [Accessed May 2, 2019].

1239 Hu F, Dan Y (2022) An inferior-superior colliculus circuit controls auditory cue-
1240 directed visual spatial attention. *Neuron* 110:109-119.e3 Available at:
1241 <https://doi.org/10.1016/j.neuron.2021.10.004> [Accessed February 8, 2024].

1242 Hupé JM, James AC, Payne BR, Lomber SG, Girard P, Bullier J (1998) Cortical
1243 feedback improves discrimination between figure and background by V1,
1244 V2 and V3 neurons. *Nature* 394:784–787 Available at:
1245 <https://www.nature.com/articles/29537> [Accessed May 19, 2021].

1246 Itaya SK, Van Hoesen GW (1982) Retinal innervation of the inferior colliculus in
1247 rat and monkey. *Brain Res* 233:45–52.

1248 Ito T, Malmierca MS (2018) Neurons, Connections, and Microcircuits of the
1249 Inferior Colliculus. In: *The Mammalian Auditory Pathways* (Oliver D, Cant
1250 N, Fay R, Popper A, eds), pp 127–167. Berlin: Springer, Cham. Available
1251 at: http://link.springer.com/10.1007/978-3-319-71798-2_6 [Accessed June
1252 2, 2018].

1253 Ito T, Ono M, Oliver DL, Ito T, Ono M, Oliver DL (2018) Neuron Types, Intrinsic
1254 Circuits, and Plasticity in the Inferior Colliculus. In: *The Oxford Handbook of*

1255 the Auditory Brainstem (Kandler K, ed). Oxford University Press. Available
1256 at:
1257 [http://oxfordhandbooks.com/view/10.1093/oxfordhb/9780190849061.001.0](http://oxfordhandbooks.com/view/10.1093/oxfordhb/9780190849061.001.001/oxfordhb-9780190849061-e-25)
1258 [001/oxfordhb-9780190849061-e-25](http://oxfordhb-9780190849061-e-25) [Accessed December 18, 2018].

1259 Jääskeläinen IP, Ahveninen J, Bonmassar G, Dale AM, Ilmoniemi RJ, Levänen
1260 S, Lin F-H, May PJC, Melcher J, Stufflebeam S, Tiitinen H, Belliveau JW
1261 (2004) Human posterior auditory cortex gates novel sounds to
1262 consciousness. *Proc Natl Acad Sci* 101:6809–6814 Available at:
1263 <http://www.pnas.org/cgi/doi/10.1073/pnas.0303760101> [Accessed June 2,
1264 2019].

1265 Jacobsen T, Horenkamp T, Schröger E (2003) Preattentive memory-based
1266 comparison of sound intensity. *Audiol Neuro-Otology* 8:338–346 Available
1267 at: <http://www.ncbi.nlm.nih.gov/pubmed/14566104> [Accessed April 23,
1268 2018].

1269 Jamal L, Khan AN, Butt S, Patel CR, Zhang H (2012) The level and distribution
1270 of the GABABR1 and GABABR2 receptor subunits in the rat's inferior
1271 colliculus. *Front Neural Circuits* 6:30930.

1272 Janacsek K, Evans TM, Kiss M, Shah L, Blumenfeld H, Ullman MT (2022)
1273 Subcortical Cognition: The Fruit Below the Rind. *Annu Rev Neurosci*
1274 45:361–386 Available at:
1275 [https://www.annualreviews.org/doi/abs/10.1146/annurev-neuro-110920-](https://www.annualreviews.org/doi/abs/10.1146/annurev-neuro-110920-013544)
1276 [013544](https://www.annualreviews.org/doi/abs/10.1146/annurev-neuro-110920-013544) [Accessed February 11, 2024].

1277 Jane JA, Masterton RB, Diamond IT (1965) The function of the tectum for
1278 attention to auditory stimuli in the cat. *J Comp Neurol* 125:165–191

1279 Available at: <https://onlinelibrary.wiley.com/doi/full/10.1002/cne.901250203>
1280 [Accessed February 8, 2024].

1281 Jen PHS, Chen QC, Sun XD (1998) Corticofugal regulation of auditory
1282 sensitivity in the bat inferior colliculus. *J Comp Physiol - A Sensory, Neural,*
1283 *Behav Physiol* 183:683–697 Available at:
1284 <https://link.springer.com/article/10.1007/s003590050291> [Accessed
1285 February 10, 2024].

1286 Keller GB, Mrsic-Flogel TD (2018) Predictive processing: a canonical cortical
1287 computation. *Neuron* 100:424–435 Available at:
1288 [https://www.sciencedirect.com/science/article/abs/pii/S0896627318308572](https://www.sciencedirect.com/science/article/abs/pii/S0896627318308572?via%3Dihub)
1289 [?via%3Dihub](https://www.sciencedirect.com/science/article/abs/pii/S0896627318308572?via%3Dihub) [Accessed June 4, 2019].

1290 King AJ, Nelken I (2009) Unraveling the principles of auditory cortical
1291 processing: can we learn from the visual system? *Nat Neurosci* 12:698–
1292 701 Available at: <http://www.nature.com/doi/10.1038/nn.2308>.

1293 Le Beau FEN, Malmierca MS, Rees A (2001) Iontophoresis in vivo
1294 demonstrates a key role for GABA(A) and glycinergic inhibition in shaping
1295 frequency response areas in the inferior colliculus of guinea pig. *J Neurosci*
1296 21:7303–7312 Available at: <http://www.ncbi.nlm.nih.gov/pubmed/11549740>
1297 [Accessed February 7, 2018].

1298 Lee T-Y, Weissenberger Y, King AJ, Dahmen JC (2024) Midbrain encodes
1299 sound detection behavior without auditory cortex.
1300 [bioRxiv:2023.06.07.544013](https://doi.org/10.1101/2023.06.07.544013) Available at:
1301 <https://www.biorxiv.org/content/10.1101/2023.06.07.544013v2> [Accessed
1302 April 3, 2024].

1303 Lesicko AMH, Angeloni CF, Blackwell JM, De Biasi M, Geffen MN (2022)
1304 Cortico-Fugal Regulation of Predictive Coding. *Elife* 11.

1305 Lesicko AMH, Geffen MN (2022) Diverse functions of the auditory cortico-
1306 collicular pathway. *Hear Res* 425:108488.

1307 Liu M, Gao Y, Xin F, Hu Y, Wang T, Xie F, Shao C, Li T, Wang N, Yuan K
1308 (2024) Parvalbumin and Somatostatin: Biomarkers for Two Parallel
1309 Tectothalamic Pathways in the Auditory Midbrain. *J Neurosci* 44 Available
1310 at: <https://www.jneurosci.org/content/44/10/e1655232024> [Accessed March
1311 30, 2024].

1312 Maggi CA, Meli A (1986) Suitability of urethane anesthesia for
1313 physiopharmacological investigations in various systems. Part 1: General
1314 considerations. *Experientia* 42:109–114 Available at:
1315 <http://www.ncbi.nlm.nih.gov/pubmed/2868911> [Accessed June 3, 2018].

1316 Malmierca MS (2015) Chapter 29 – Auditory System. In: *The Rat Nervous*
1317 *System* (Paxinos G, ed), pp 865–946. Cambridge: Academic Press.
1318 Available at:
1319 <http://www.sciencedirect.com/science/article/pii/B9780123742452000292>
1320 [Accessed April 3, 2017].

1321 Malmierca MS, Carbajal G V., Escera C (2019) Deviance Detection and
1322 Encoding Acoustic Regularity in the Auditory Midbrain. In: *The Oxford*
1323 *Handbook of the Auditory Brainstem* (Kandler K, ed), pp 706–740. Oxford
1324 University Press. Available at:
1325 [http://oxfordhandbooks.com/view/10.1093/oxfordhb/9780190849061.001.0](http://oxfordhandbooks.com/view/10.1093/oxfordhb/9780190849061.001.001/oxfordhb-9780190849061-e-19)
1326 [001/oxfordhb-9780190849061-e-19](http://oxfordhandbooks.com/view/10.1093/oxfordhb/9780190849061.001.001/oxfordhb-9780190849061-e-19) [Accessed September 19, 2019].

1327 Malmierca MS, Cristaudo S, Pérez-González D, Covey E (2009) Stimulus-
1328 Specific Adaptation in the Inferior Colliculus of the Anesthetized Rat. *J*
1329 *Neurosci* 29:5483–5493 Available at:
1330 <http://www.jneurosci.org/cgi/doi/10.1523/JNEUROSCI.4153-08.2009>.

1331 Malmierca MS, Ryugo DK (2011) Descending connections of auditory cortex to
1332 the midbrain and brain stem. In: *The Auditory Cortex*, 1st ed. (Winer JA,
1333 Schreiner CE, eds), pp 189–208. Boston, MA: Springer US. Available at:
1334 http://link.springer.com/10.1007/978-1-4419-0074-6_9 [Accessed
1335 September 20, 2017].

1336 Merchán MA, Aguilar LA, Lopez-Poveda EA, Malmierca MS (2005) The inferior
1337 colliculus of the rat: Quantitative immunocytochemical study of GABA and
1338 glycine. *Neuroscience* 136:907–925 Available at:
1339 <https://www.sciencedirect.com/science/article/pii/S0306452205000564>
1340 [Accessed February 4, 2018].

1341 Merrill EG, Ainsworth A (1972) Glass-coated platinum-plated tungsten
1342 microelectrodes. *Med Biol Eng* 10:662–672 Available at:
1343 <http://link.springer.com/10.1007/BF02476084> [Accessed February 7, 2018].

1344 Metzger RR, Greene NT, Porter KK, Groh JM (2006) Effects of reward and
1345 behavioral context on neural activity in the primate inferior colliculus. *J*
1346 *Neurosci* 26:7468–7476 Available at:
1347 <https://www.jneurosci.org/content/26/28/7468> [Accessed February 8, 2024].

1348 Michel MM, Chen Y, Seidemann E, Geisler WS (2018) Nonlinear Lateral
1349 Interactions in V1 Population Responses Explained by a Contrast Gain
1350 Control Model. *J Neurosci* 38:10069–10079.

- 1351 Milbrandt JC, Albin RL, Turgeon SM, Caspary DM (1996) GABAA receptor
1352 binding in the aging rat inferior colliculus. *Neuroscience* 73:449–458.
- 1353 Mill RW, Coath M, Wennekers T, Denham SL (2011) A neurocomputational
1354 model of stimulus-specific adaptation to oddball and markov sequences
1355 Sporns O, ed. *PLoS Comput Biol* 7:e1002117 Available at:
1356 <https://dx.plos.org/10.1371/journal.pcbi.1002117> [Accessed December 12,
1357 2018].
- 1358 Mitani A, Shimokouchi M, Nomura S (1983) Effects of stimulation of the primary
1359 auditory cortex upon colliculogeniculate neurons in the inferior colliculus of
1360 the cat. *Neurosci Lett* 42:185–189.
- 1361 Nelken I, Fishbach A, Las L, Ulanovsky N, Farkas D (2003) Primary auditory
1362 cortex of cats: Feature detection or something else? *Biol Cybern* 89:397–
1363 406 Available at: [https://link.springer.com/article/10.1007/s00422-003-](https://link.springer.com/article/10.1007/s00422-003-0445-3)
1364 [0445-3](https://link.springer.com/article/10.1007/s00422-003-0445-3) [Accessed February 8, 2024].
- 1365 Nieto-Diego J, Malmierca MS (2016) Topographic Distribution of Stimulus-
1366 Specific Adaptation across Auditory Cortical Fields in the Anesthetized Rat.
1367 *PLoS Biol* 14:e1002397 Available at:
1368 <http://dx.doi.org/10.1371/journal.pbio.1002397>.
- 1369 Nwabueze-Ogbo FC, Popelář J, Syka J (2003) Changes in Neuronal Activity of
1370 the Inferior Colliculus in Rat after Temporal Inactivation of the Auditory
1371 Cortex. *Physiol Res* 52:615–628 Available at:
1372 <http://www.biomed.cas.cz/physiolres> [Accessed May 22, 2021].
- 1373 Oliver D, Cant N, Fay R, Popper Editors A (2017) *The Mammalian Auditory*
1374 *Pathways: synaptic organization and microcircuits*. Springer. Available at:

1375 <http://www.springer.com/series/2506>.

1376 Oliver DL (2005) Neuronal organization in the inferior colliculus. In: *The Inferior*
1377 *Colliculus*, pp 69–114. Springer New York. Available at:
1378 https://link.springer.com/chapter/10.1007/0-387-27083-3_2 [Accessed May
1379 13, 2021].

1380 Olthof BMJ, Rees A, Gartside SE (2019) Multiple nonauditory cortical regions
1381 innervate the auditory midbrain. *J Neurosci* 39:8916–8928 Available at:
1382 <https://www.jneurosci.org/content/39/45/8916> [Accessed April 13, 2023].

1383 Palmer AR, Shackleton TM, Sumner CJ, Zobay O, Rees A (2013) Classification
1384 of frequency response areas in the inferior colliculus reveals continua not
1385 discrete classes. *J Physiol* 591:4003–4025 Available at:
1386 <https://onlinelibrary.wiley.com/doi/full/10.1113/jphysiol.2013.255943>
1387 [Accessed September 27, 2022].

1388 Parras GG, Casado-Román L, Schröger E, Malmierca MS (2021) The posterior
1389 auditory field is the chief generator of prediction error signals in the auditory
1390 cortex. *Neuroimage* 242:118446.

1391 Parras GG, Nieto-Diego J, Carbajal G V., Valdés-Baizabal C, Escera C,
1392 Malmierca MS (2017) Neurons along the auditory pathway exhibit a
1393 hierarchical organization of prediction error. *Nat Commun* 8:2148 Available
1394 at: <http://dx.doi.org/10.1038/s41467-017-02038-6>.

1395 Parvizi J (2009) Corticocentric myopia: old bias in new cognitive sciences.
1396 *Trends Cogn Sci* 13:354–359.

1397 Paxinos G, Watson C (2007) *The rat brain in stereotaxic coordinates*.

- 1398 Cambridge: Academic Press.
- 1399 Peng F, Harper NS, Mishra AP, Auksztulewicz R, Schnupp JWH (2024)
1400 Dissociable Roles of the Auditory Midbrain and Cortex in Processing the
1401 Statistical Features of Natural Sound Textures. *J Neurosci* 44 Available at:
1402 <https://www.jneurosci.org/content/44/10/e1115232023> [Accessed March
1403 30, 2024].
- 1404 Pérez-González D, Malmierca MS, Covey E (2005) Novelty detector neurons in
1405 the mammalian auditory midbrain. *Eur J Neurosci* 22:2879–2885 Available
1406 at: <http://doi.wiley.com/10.1111/j.1460-9568.2005.04472.x> [Accessed
1407 September 12, 2017].
- 1408 Pérez-González D, Parras GG, Morado-Díaz CJ, Aedo-Sánchez C, Carbajal G
1409 V., Malmierca MS (2021) Deviance detection in physiologically identified
1410 cell types in the rat auditory cortex. *Hear Res* 399:107997.
- 1411 Peter V, McArthur G, Thompson WF (2010) Effect of deviance direction and
1412 calculation method on duration and frequency mismatch negativity (MMN).
1413 *Neurosci Lett* 482:71–75.
- 1414 Polley DB, Read HL, Storace DA, Merzenich MM (2007) Multiparametric
1415 Auditory Receptive Field Organization Across Five Cortical Fields in the
1416 Albino Rat. *J Neurophysiol* 97:3621–3638 Available at:
1417 <http://jn.physiology.org/cgi/doi/10.1152/jn.01298.2006>.
- 1418 Popelář J, Šuta D, Lindovský J, Bureš Z, Pysanenko K, Chumak T, Syka J
1419 (2016) Cooling of the auditory cortex modifies neuronal activity in the
1420 inferior colliculus in rats. *Hear Res* 332:7–16.

1421 Porter KK, Metzger RR, Groh JM (2007) Visual- and saccade-related signals in
1422 the primate inferior colliculus. *Proc Natl Acad Sci U S A* 104:17855–17860
1423 Available at: <https://www.pnas.org/doi/abs/10.1073/pnas.0706249104>
1424 [Accessed February 8, 2024].

1425 Quass GL, Rogalla MM, Ford AN, Apostolides PF (2023) Mixed representations
1426 of sound and action in the auditory midbrain. *bioRxiv* Available at:
1427 [/pmc/articles/PMC10541616/](https://www.ncbi.nlm.nih.gov/pmc/articles/PMC10541616/) [Accessed April 2, 2024].

1428 Rao RPN, Ballard DH (1999) Predictive coding in the visual cortex: a functional
1429 interpretation of some extra-classical receptive-field effects. *Nat Neurosci*
1430 2:79–87 Available at:
1431 [10.1038/4580%5Cnhttp://www.nature.com/neuro/journal/v2/n1/abs/nn0199](http://www.nature.com/neuro/journal/v2/n1/abs/nn0199_79.html)
1432 [_79.html](http://www.nature.com/neuro/journal/v2/n1/abs/nn0199_79.html).

1433 Rinne T, Balk MH, Koistinen S, Autti T, Alho K, Sams M (2008) Auditory
1434 selective attention modulates activation of human inferior colliculus. *J*
1435 *Neurophysiol* 100:3323–3327 Available at:
1436 <https://journals.physiology.org/doi/10.1152/jn.90607.2008> [Accessed
1437 February 8, 2024].

1438 Ruhnau P, Herrmann B, Schröger E (2012) Finding the right control: The
1439 mismatch negativity under investigation. *Clin Neurophysiol* 123:507–512.

1440 Ryan A, Miller J (1977) Effects of behavioral performance on single unit firing
1441 patterns in inferior colliculus of the rhesus monkey. *J Neurophysiol* 40:943–
1442 956 Available at:
1443 <https://journals.physiology.org/doi/10.1152/jn.1977.40.4.943> [Accessed
1444 February 8, 2024].

1445 Sceniak MP, Maclver MB (2006) Cellular Actions of Urethane on Rat Visual
1446 Cortical Neurons In Vitro. *J Neurophysiol* 95:3865–3874 Available at:
1447 <http://www.physiology.org/doi/10.1152/jn.01196.2005> [Accessed June 3,
1448 2018].

1449 Schelinski S, Tabas A, von Kriegstein K (2022) Altered processing of
1450 communication signals in the subcortical auditory sensory pathway in
1451 autism. *Hum Brain Mapp* 43:1955–1972 Available at:
1452 <https://onlinelibrary.wiley.com/doi/full/10.1002/hbm.25766> [Accessed
1453 February 9, 2024].

1454 Schneider F, Balezeau F, Distler C, Kikuchi Y, van Kempen J, Gieselmann A,
1455 Petkov CI, Thiele A, Griffiths TD (2021) Neuronal figure-ground responses
1456 in primate primary auditory cortex. *Cell Rep* 35:109242.

1457 Schneider F, Dheerendra P, Balezeau F, Ortiz-Rios M, Kikuchi Y, Petkov CI,
1458 Thiele A, Griffiths TD (2018) Auditory figure-ground analysis in rostral belt
1459 and parabelt of the macaque monkey. *Sci Rep* 8:1–8 Available at:
1460 <https://www.nature.com/articles/s41598-018-36903-1> [Accessed February
1461 12, 2024].

1462 Schofield BR, Beebe NL (2019) Descending Auditory Pathways and Plasticity.
1463 In: *The Oxford Handbook of the Auditory Brainstem*, pp 610–638. Oxford
1464 University Press. Available at:
1465 [https://www.oxfordhandbooks.com/view/10.1093/oxfordhb/9780190849061.
1466 001.0001/oxfordhb-9780190849061-e-17](https://www.oxfordhandbooks.com/view/10.1093/oxfordhb/9780190849061.001.0001/oxfordhb-9780190849061-e-17) [Accessed May 13, 2021].

1467 Schreiner CE, Langner G (1997) Laminar fine structure of frequency
1468 organization in auditory midbrain. *Nature* 388:383–386 Available at:

1469 <https://www.nature.com/articles/41106> [Accessed February 18, 2024].

1470 Schröger E, Wolff C (1996) Mismatch response of the human brain to changes
1471 in sound location. *Neuroreport* 7:3005–3008 Available at:
1472 <http://www.ncbi.nlm.nih.gov/pubmed/9116228> [Accessed February 4,
1473 2018].

1474 Slabu L, Grimm S, Escera C (2012) Novelty detection in the human auditory
1475 brainstem. *J Neurosci* 32:1447–1452.

1476 Stefanics G, Kremláček J, Czigler I (2014) Visual mismatch negativity: a
1477 predictive coding view. *Front Hum Neurosci* 8:666 Available at:
1478 <http://journal.frontiersin.org/article/10.3389/fnhum.2014.00666/abstract>.

1479 Taaseh N, Yaron A, Nelken I (2011) Stimulus-Specific Adaptation and Deviance
1480 Detection in the Rat Auditory Cortex Sugihara I, ed. *PLoS One* 6:e23369
1481 Available at: <http://dx.plos.org/10.1371/journal.pone.0023369> [Accessed
1482 October 29, 2017].

1483 Tabas A, Mihai G, Kiebel S, Trampel R, Von Kriegstein K (2020) Abstract rules
1484 drive adaptation in the subcortical sensory pathway. *Elife* 9:1–19.

1485 Tabas A, von Kriegstein K (2021) Adjudicating Between Local and Global
1486 Architectures of Predictive Processing in the Subcortical Auditory Pathway.
1487 *Front Neural Circuits* 15.

1488 Tabas A, von Kriegstein K (2024) Multiple concurrent predictions inform
1489 prediction error in the human auditory pathway. *J Neurosci* 44:JN-RM-
1490 2219-22 Available at: <https://www.jneurosci.org/content/44/1/e2219222023>
1491 [Accessed February 9, 2024].

1492 Tawil RN, Saadé NE, Bitar M, Jabbur SJ (1983) Polysensory interactions on
1493 single neurons of cat inferior colliculus. *Brain Res* 269:149–152.

1494 Tervaniemi M, Maury S, Näätänen R (1994) Neural representations of abstract
1495 stimulus features in the human brain as reflected by the mismatch
1496 negativity. *Neuroreport* 5:844–846 Available at:
1497 <http://www.ncbi.nlm.nih.gov/pubmed/8018861> [Accessed February 1,
1498 2018].

1499 Thompson GC, Masterton RB (1978) Brain stem auditory pathways involved in
1500 reflexive head orientation to sound. *J Neurophysiol* 41:1183–1202
1501 Available at: <https://journals.physiology.org/doi/10.1152/jn.1978.41.5.1183>
1502 [Accessed February 8, 2024].

1503 Todorovic A, de Lange FP (2012) Repetition suppression and expectation
1504 suppression are dissociable in time in early auditory evoked fields. *J*
1505 *Neurosci* 32:13389–13395 Available at:
1506 <http://www.ncbi.nlm.nih.gov/pubmed/23015429> [Accessed April 27, 2018].

1507 Tokunaga A, Sugita S, Otani K (1984) Auditory and non-auditory subcortical
1508 afferents to the inferior colliculus in the rat. *J Hirnforsch* 25:461–472
1509 Available at: <https://europepmc.org/article/med/6481158> [Accessed May
1510 19, 2021].

1511 Ulanovsky N, Las L, Nelken I (2003) Processing of low-probability sounds by
1512 cortical neurons. *Nat Neurosci* 6:391–398 Available at:
1513 <https://search.proquest.com/docview/230485606?pq-origsite=gscholar>
1514 [Accessed September 12, 2017].

1515 Valdés-Baizabal C, Carbajal G V., Pérez-González D, Malmierca MS (2020)

1516 Dopamine modulates subcortical responses to surprising sounds. PLoS
1517 Biol 18:e3000744 Available at: <https://doi.org/10.1371/journal.pbio.3000744>
1518 [Accessed September 3, 2020].

1519 Vila CH, Williamson RS, Hancock KE, Polley DB (2019) Optimizing optogenetic
1520 stimulation protocols in auditory corticofugal neurons based on closed-loop
1521 spike feedback. J Neural Eng 16:066023 Available at:
1522 <https://iopscience.iop.org/article/10.1088/1741-2552/ab39cf> [Accessed
1523 February 10, 2024].

1524 Wiens S, Szychowska M, Eklund R, van Berlekom E (2019) Cascade and no-
1525 repetition rules are comparable controls for the auditory frequency
1526 mismatch negativity in oddball tasks. Psychophysiology 56:e13280
1527 Available at: <https://onlinelibrary.wiley.com/doi/abs/10.1111/psyp.13280>
1528 [Accessed May 30, 2019].

1529 Winer JA, Chernock ML, Larue DT, Cheung SW (2002) Descending projections
1530 to the inferior colliculus from the posterior thalamus and the auditory cortex
1531 in rat, cat, and monkey. Hear Res 168:181–195.

1532 Zhao L, Liu Y, Shen L, Feng L, Hong B (2011) Stimulus-specific adaptation and
1533 its dynamics in the inferior colliculus of rat. Neuroscience 181:163–174
1534 Available at: <http://dx.doi.org/10.1016/j.neuroscience.2011.01.060>.

1535 Zhou X, Jen PHS (2005) Corticofugal modulation of directional sensitivity in the
1536 midbrain of the big brown bat, *Eptesicus fuscus*. Hear Res 203:201–215.

1537 Zwiers MP, Versnel H, Van Opstal AJ (2004) Involvement of Monkey Inferior
1538 Colliculus in Spatial Hearing. J Neurosci 24:4145–4156 Available at:
1539 <https://www.jneurosci.org/content/24/17/4145> [Accessed February 8, 2024].

1542 **FIGURES**

1543

1544 **Figure 1.** Experimental design. **(A)** Three possible experimental conditions within
1545 an oddball paradigm for a given tone of interest f_i (colored). **(B)** Three possible
1546 control conditions set by the MSC and CAS for a given tone of interest f_i (in
1547 green). **(C)** Schematic representation of an experimental setup for in vivo
1548 extracellular recording of auditory-evoked responses in a rat brain, depicting the
1549 neuroanatomical features most relevant to this paper. **(D)** Decomposition of
1550 neuronal mismatch responses using the controls and quantification in 3 indices.

JNeurosci Accepted Manuscript

1551

1552 **Figure 2.** IC processing of control sequences. **(A)** Schematic representation of
1553 frequency step comparisons. Responses to extreme step values featuring in both
1554 MSC and CAS, i.e., 0.5-octave and 4.5-octave steps, are compared across
1555 control sequences (highlighted and framed in green). Responses to different
1556 frequency steps (0.5, 1.0, 1.5, 2.0, 2.5, 3.0, 3.5, 4.0, or 4.5 octaves) within the
1557 MSC are also compared. **(B-C)** Comparison matrices showing the differences in
1558 the evoked spiking responses after different frequency steps presented within the
1559 MSC or the CAS in lemniscal and nonlemniscal divisions of the IC. The
1560 normalized mean difference between the spikes per trial in the x-axis minus those
1561 in the y-axis is noted as a percentage where statistical significances were found
1562 (ANOVA, $p < 0.05$, highlighted in green). Significant differences found in both
1563 lemniscal and nonlemniscal divisions of the IC are marked as underlined digits,
1564 all corresponding to comparisons between 4.5-octave steps in CAS with the rest
1565 of smaller steps. Two circles in each matrix mark equal step comparisons across
1566 control sequences. **(B)** The lemniscal IC better distinguished different frequency
1567 steps (note the many significant green squares) and responded similarly to equal
1568 frequency steps happening in different controls (black dotted circles). **(C)** The
1569 nonlemniscal IC did not perform this spectral processing but could instead
1570 differentiate between equal frequency steps presented in different sequences
1571 (white circles).

1572

1573

1574 **Figure 3.** Prediction error as a function of intensity and direction of frequency
1575 change in four auditory regions that engage in predictive processing. **(A)** Linear
1576 models fitted for the iPE (calculated with CAS or MSC) using dB SPL and
1577 direction of frequency change (ascending or descending) as predictors. Error
1578 bars denote mean and standard error of the mean for each intensity level and
1579 direction. The only models that achieved a statistically significant adjustment
1580 were in the nonlemniscal IC (first plot), revealing a clear tendency to show higher
1581 iPE values at lower intensities. **(B)** Violin plots comparing the spike counts evoked
1582 by DEV (in red) and CAS (in green) at low intensities (< 40 dB SPL, left violin)
1583 and high intensities (\geq 40 dB SPL, right violin).

1584

JNeurosci Accepted Manuscript

1585

1586

1587 **Figure 4.** Prediction error as a function of intensity and direction of frequency
1588 change in four types of FRA. **(A)** Categories of FRA shapes recorded in the
1589 nonlemniscal IC. **(B)** Linear models fitted for the iPE using dB SPL and direction
1590 (ascending or descending) as predictors. Error bars denote mean and standard
1591 error of the mean for each SPL and direction. The only models that did not
1592 achieve a statistically significant adjustment were those of the neurons that
1593 exhibited mosaic FRAs (fourth plot). Note that these neurons tended to show high
1594 iPE values, regardless of the intensity or direction of frequency change. **(C)** Violin
1595 plots comparing the spike counts evoked by DEV (in red) and CAS (in green) at
1596 low intensities (< 40 dB SPL, left violin) and high intensities (≥ 40 dB SPL, right
1597 violin). Note how the category of mosaic FRAs (fourth plot) completely deviates
1598 from the rest.

1599

1600 **Figure 5.** Time course of iPE (in orange) and iRS (in cyan) for each FRA type.

1601 **(A)** Categories of FRA shapes recorded in the nonlemniscal IC. **(B)** Time course

1602 of the iPE and iRS (mean \pm standard error of the mean) when the intensity of

1603 stimulation was low (< 40 dB SPL). Black asterisks mark a significant value ($p <$

1604 0.05 , Wilcoxon signed-rank test, FDR-corrected for 8 comparisons) for the

1605 corresponding time window of 20 ms. Note that all but sharply tuned neurons (V,

1606 first plot) showed significant traces of PE signaling at low intensity stimulation.

1607 **(C)** Time course of the average iPE and iRS when the stimulation intensity was

1608 high (≥ 40 dB SPL). Note that whereas the iRS prevails largely unchanged across

1609 all categories, only the untuned neurons showing mosaic FRAs preserved their

1610 iPE values at high intensity stimulation (fourth plot).

1611

1612

1613

1614 **Figure 6.** Summary of results. **(A)** Median iPE (orange) and iRS (cyan) of each
1615 FRA category recorded in the nonlemniscal IC, represented with respect to the
1616 baseline set by CAS (green horizontal bar), at low and high intensity stimulation
1617 (left and right plots, respectively). Thereby, iPE is upwards-positive while iRS is
1618 downwards-positive (see Figure 1B). Striped regions in the bars mark negative
1619 iPE values. Asterisks denote statistical significance of the indices against zero:
1620 *n.s.*, nonsignificant, $*p < 0.05$, $**p < 0.01$, $***p < 0.001$. **(B)** Median iPE and iRS of
1621 each FRA category represented with respect to the baseline set by MSC (green
1622 horizontal bar).

1623

1624

1625 **Figure 7.** Early emergence of predictive processing in the auditory system. **(A-**
1626 **B)** Comparison matrices for, respectively, the nonlemniscal AC and the group of
1627 X-neurons in the nonlemniscal IC, setting X-neurons apart from the rest of
1628 nonlemniscal IC neurons (cf. Figure 2C) and implying a functional connection
1629 between both neural substrates. **(C)** Schematics of connectivity between the IC,
1630 MGB and AC. Descending projections targeting the nonlemniscal pathway
1631 extend the hierarchical exchange of predictions and prediction errors to earlier
1632 stages of auditory processing, presumably improving its overall efficiency. **(D)**
1633 Diagram summarizing our proposed classification of neuronal and functional
1634 elements in the intrinsic circuitry of the IC. 'Raw' spectral information from the
1635 central nucleus flows into the predictive processing circuitry of the IC cortices via
1636 V-neurons, which constitute the first filter of redundant input. Once at the

1637 beginning of the nonlemniscal pathway, unexpected input will be consistently
1638 reported to higher-order processing levels by the 'non-spectral' PE system
1639 constituted by X-neurons with untuned receptive fields. When a deviant sound is
1640 close to the hearing threshold or is moving to a higher pitch, unexpected input
1641 additionally benefit from dynamic gain compensation provided by the 'spectral'
1642 PE system formed by W- and U-neurons with broad receptive fields.

1643

1644

JNeurosci Accepted Manuscript

1645 **TABLES**

1646 **Table 1.** Median normalized spike counts and indices calculated using CAS in
 1647 each auditory region and at different intensities of stimulation. Significant iPE
 1648 values are highlighted in bold (Friedman test).

ALL INTENSITIES	IC		MGB		AC	
	Lem.	Nonlem.	Lem.	Nonlem.	Lem.	Nonlem.
Units	70	204	41	52	97	49
Tones	616	1711	183	364	586	407
DEV	0.589	0.661	0.591	0.684	0.745	0.795
STD	0.432	0.225	0.241	0.162	0.159	0.175
CAS	0.647	0.640	0.672	0.627	0.570	0.495
iMM	0.156	0.436	0.350	0.522	0.586	0.620
<i>p value</i>	0.000	0.000	0.000	0.000	0.000	0.000
iPE	-0.058	0.021	-0.081	0.057	0.175	0.301
<i>p value</i>	0.008	0.007	0.271	0.006	0.000	0.000
iRS	0.214	0.415	0.431	0.465	0.412	0.319
<i>p value</i>	0.000	0.000	0.000	0.000	0.000	0.000
LOW INTENSITIES (< 40 dB SPL)	Lem.	Nonlem.	Lem.	Nonlem.	Lem.	Nonlem.
Units	33	79	7	14	33	11
Tones	161	468	20	61	168	65
DEV	0.624	0.716	0.533	0.688	0.724	0.790
STD	0.455	0.160	0.173	0.147	0.144	0.257

CAS	0.609	0.596	0.743	0.669	0.604	0.435
iMM	0.169	0.556	0.359	0.541	0.580	0.533
p value	0.000	0.000	0.003	0.000	0.000	0.000
iPE	0.014	0.120	-0.211	0.019	0.120	0.355
p value	0.094	0.000	0.426	0.464	0.113	0.000
iRS	0.154	0.436	0.570	0.522	0.461	0.178
p value	0.000	0.000	0.000	0.000	0.000	0.007
HIGH INTENSITIES (≥ 40 dB SPL)	Lem.	Nonlem.	Lem.	Nonlem.	Lem.	Nonlem.
Units	63	171	36	46	74	46
Tones	455	1243	163	303	418	342
DEV	0.581	0.643	0.600	0.682	0.750	0.799
STD	0.428	0.252	0.273	0.164	0.166	0.163
CAS	0.654	0.656	0.660	0.612	0.553	0.519
iMM	0.153	0.391	0.327	0.518	0.583	0.636
p value	0.000	0.000	0.000	0.000	0.000	0.000
iPE	-0.074	-0.014	-0.060	0.070	0.197	0.280
p value	0.000	0.507	0.375	0.008	0.000	0.000
iRS	0.227	0.405	0.387	0.448	0.386	0.356
p value	0.000	0.000	0.000	0.000	0.000	0.000

1650 **Table 2.** Median normalized spike counts and indices calculated using MSC in
 1651 each auditory region and at different intensities of stimulation. Significant iPE
 1652 values are highlighted in bold (Friedman test).

ALL INTENSITIES	IC		MGB		AC	
	Lem.	Nonlem.	Lem.	Nonlem.	Lem.	Nonlem.
Units	70	235	53	96	103	57
Tones	614	1912	214	569	635	465
DEV	0.586	0.659	0.615	0.669	0.714	0.770
STD	0.424	0.191	0.302	0.189	0.164	0.177
MSC	0.646	0.657	0.659	0.634	0.627	0.541
iMM	0.162	0.468	0.313	0.480	0.550	0.592
<i>p value</i>	0.000	0.000	0.000	0.000	0.000	0.000
iPE	-0.060	0.002	-0.044	0.035	0.087	0.229
<i>p value</i>	0.000	0.686	0.371	0.467	0.005	0.000
iRS	0.222	0.465	0.357	0.445	0.463	0.364
<i>p value</i>	0.000	0.000	0.000	0.000	0.000	0.000
LOW INTENSITIES (< 40 dB SPL)	Lem.	Nonlem.	Lem.	Nonlem.	Lem.	Nonlem.
Units	32	98	6	42	39	16
Tones	160	531	18	114	195	97
DEV	0.611	0.707	0.724	0.679	0.726	0.708
STD	0.440	0.151	0.193	0.193	0.161	0.236
MSC	0.591	0.620	0.625	0.607	0.599	0.615
iMM	0.171	0.556	0.531	0.486	0.565	0.472

<i>p value</i>	0.000	0.000	0.000	0.000	0.000	0.000
iPE	0.020	0.087	0.099	0.072	0.127	0.094
<i>p value</i>	0.218	0.001	0.617	0.162	0.027	0.085
iRS	0.151	0.468	0.432	0.414	0.438	0.379
<i>p value</i>	0.000	0.000	0.003	0.000	0.000	0.000
HIGH INTENSITIES (≥ 40 dB SPL)	Lem.	Nonlem.	Lem.	Nonlem.	Lem.	Nonlem.
Units	63	196	49	91	80	51
Tones	454	1381	196	455	440	368
DEV	0.159	0.642	0.593	0.659	0.712	0.791
STD	-0.080	0.221	0.318	0.186	0.165	0.172
MSC	0.238	0.666	0.661	0.640	0.635	0.514
iMM	0.238	0.420	0.275	0.473	0.547	0.619
<i>p value</i>	0.000	0.000	0.000	0.000	0.000	0.000
iPE	-0.080	-0.025	-0.068	0.019	0.076	0.277
<i>p value</i>	0.000	0.014	0.277	0.908	0.059	0.000
iRS	0.318	0.445	0.342	0.454	0.470	0.342
<i>p value</i>	0.000	0.000	0.000	0.000	0.000	0.000

1653

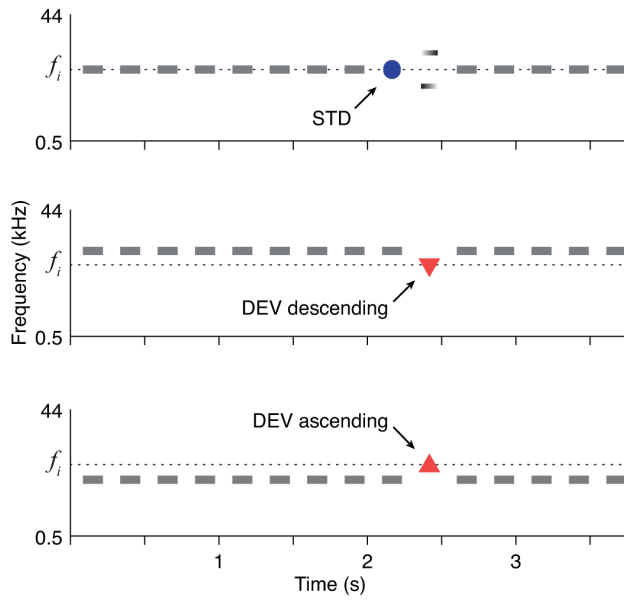
1654 **Table 3.** Median indices calculated using both controls for each FRA category
 1655 recorded in the nonlemniscal IC. Significant iPE values are highlighted in bold
 1656 (Friedman test).

	CAS				MSC			
ALL INTENSITIES	V	W	U	X	V	W	U	X
Units	54	44	62	44	61	50	76	48
Tones	375	535	484	317	406	578	587	341
iMM	0.225	0.467	0.501	0.532	0.231	0.481	0.543	0.501
<i>p value</i>	0.000	0.000	0.000	0.000	0.000	0.000	0.000	0.000
iPE	-0.019	-0.014	-0.010	0.214	-0.052	-0.012	-0.010	0.146
<i>p value</i>	0.660	0.571	0.676	0.000	0.012	0.133	0.189	0.000
iRS	0.244	0.480	0.511	0.318	0.283	0.492	0.553	0.355
<i>p value</i>	0.000	0.000	0.000	0.000	0.000	0.000	0.000	0.000
LOW INTENSITIES (< 40 dB SPL)	V	W	U	X	V	W	U	X
Units	20	20	24	15	24	23	33	18
Tones	87	151	119	111	96	163	147	125
iMM	0.225	0.467	0.501	0.532	0.346	0.583	0.648	0.545
<i>p value</i>	0.000	0.000	0.000	0.000	0.000	0.000	0.000	0.000
iPE	0.039	0.107	0.114	0.230	-0.006	0.063	0.098	0.166
<i>p value</i>	0.110	0.000	0.003	0.000	0.427	0.256	0.017	0.000
iRS	0.300	0.485	0.530	0.282	0.352	0.520	0.551	0.379
<i>p value</i>	0.000	0.000	0.000	0.000	0.000	0.000	0.000	0.000

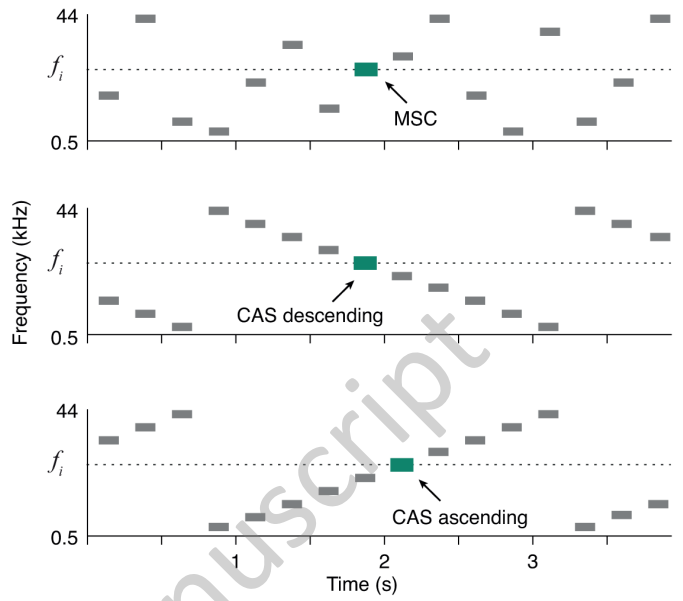
HIGH INTENSITIES (≥ 40 dB SPL)	V	W	U	X	V	W	U	X
Units	46	39	52	34	52	45	63	36
Tones	288	384	365	206	310	415	440	216
iMM	0.202	0.404	0.455	0.539	0.210	0.444	0.504	0.482
<i>p value</i>	<i>0.000</i>	<i>0.000</i>	<i>0.000</i>	<i>0.000</i>	<i>0.000</i>	<i>0.000</i>	<i>0.000</i>	<i>0.000</i>
iPE	-0.032	-0.051	-0.048	0.218	-0.063	-0.034	-0.042	0.132
<i>p value</i>	<i>0.707</i>	<i>0.006</i>	<i>0.028</i>	<i>0.000</i>	<i>0.015</i>	<i>0.013</i>	<i>0.004</i>	<i>0.000</i>
iRS	0.233	0.454	0.502	0.321	0.273	0.478	0.546	0.350
<i>p value</i>	<i>0.000</i>	<i>0.000</i>	<i>0.000</i>	<i>0.000</i>	<i>0.000</i>	<i>0.000</i>	<i>0.000</i>	<i>0.000</i>

1657

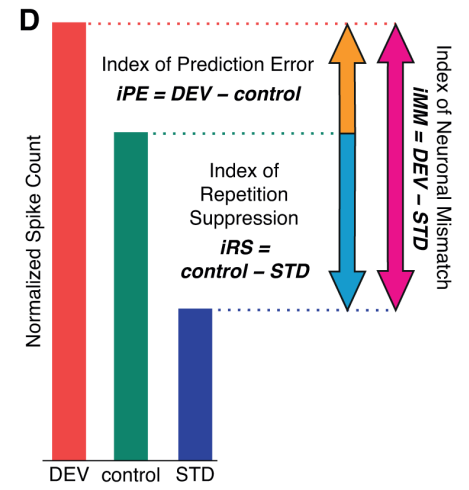
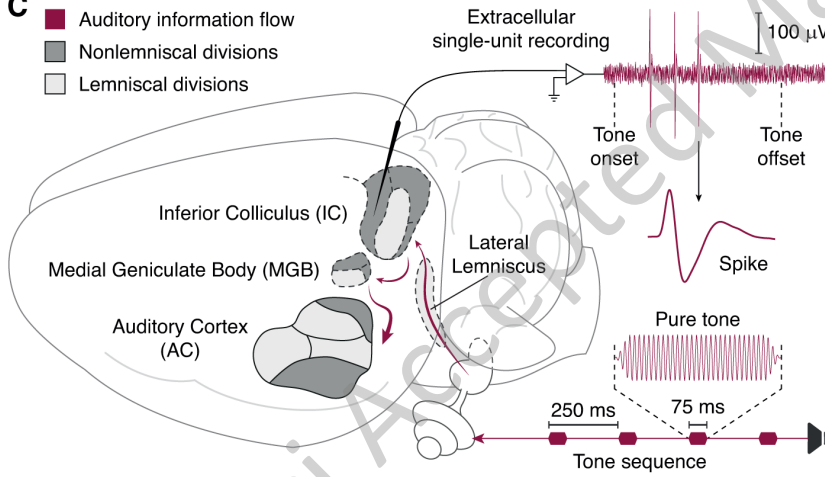
A Oddball paradigm conditions

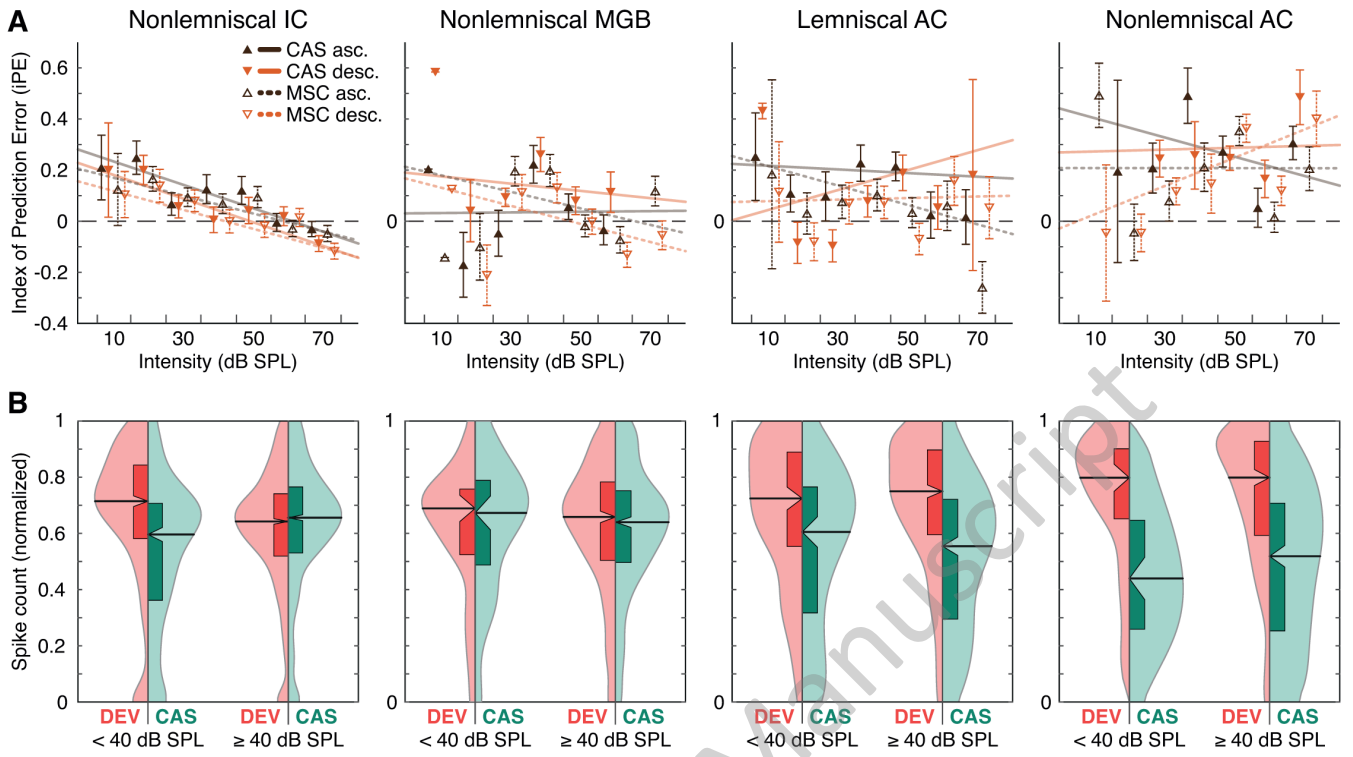


B Control conditions

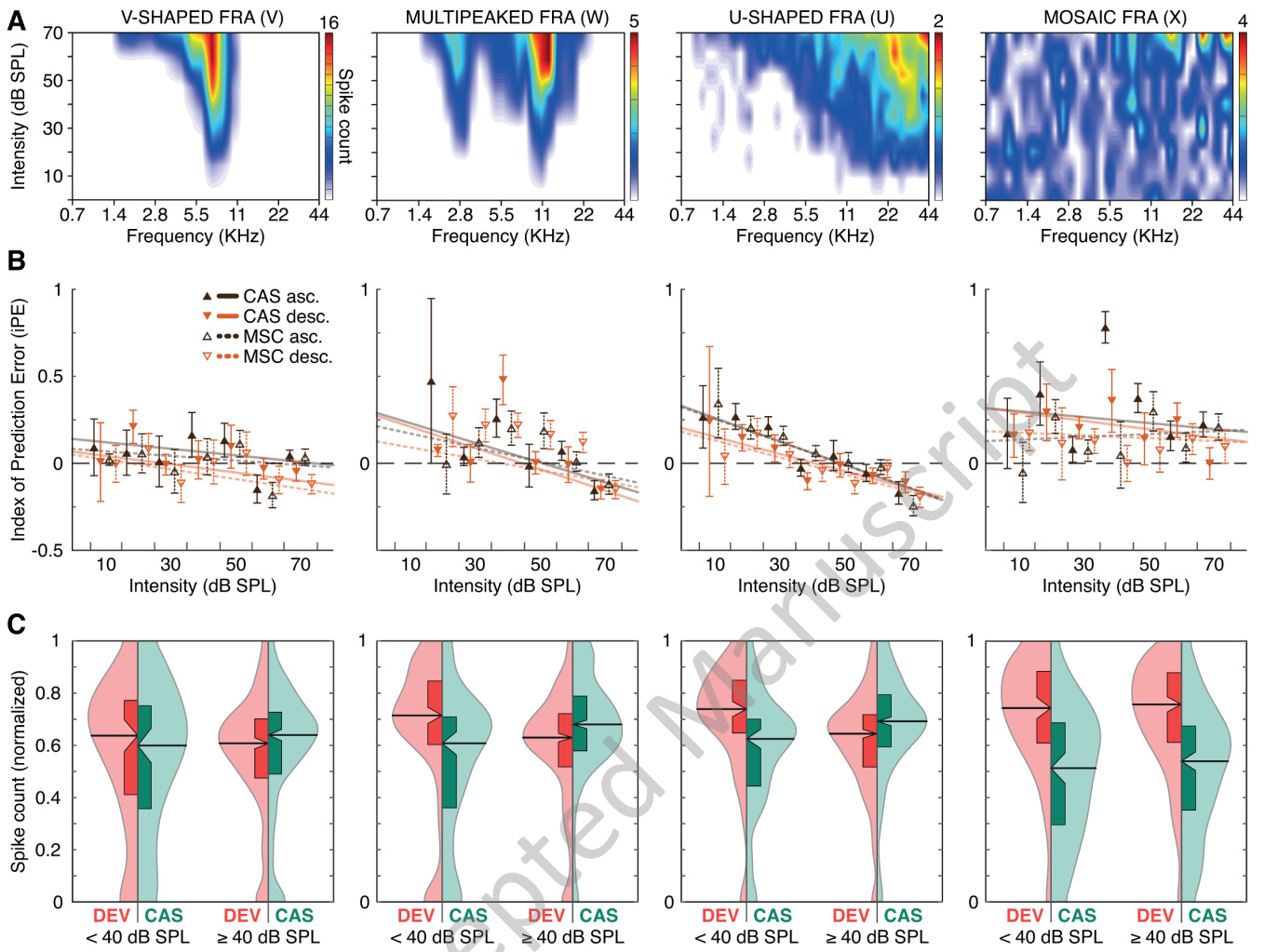


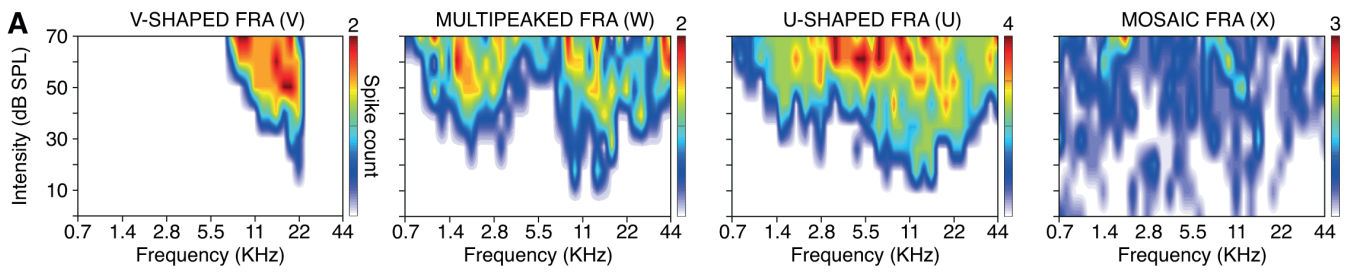
- Auditory information flow
- Nonlemniscal divisions
- Lemniscal divisions



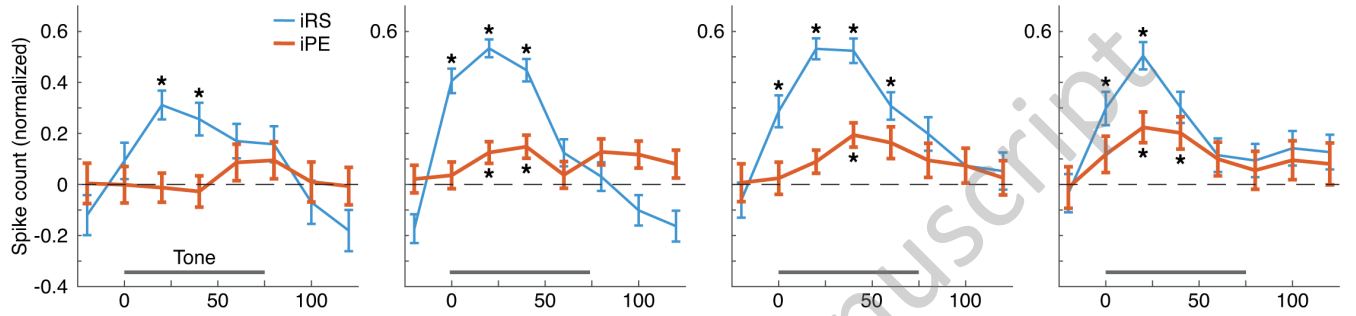


JNeurosci Accepted Manuscript

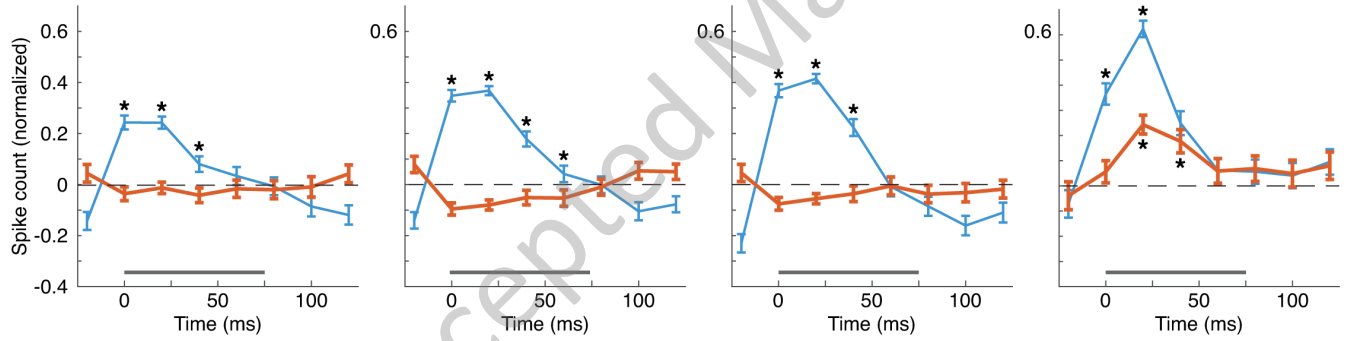




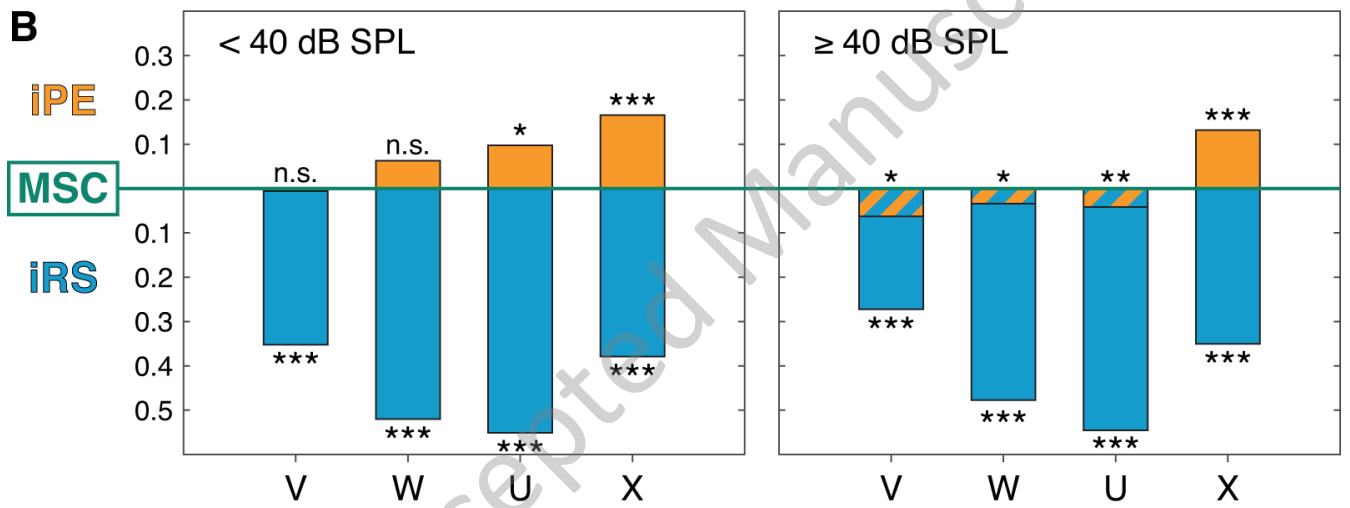
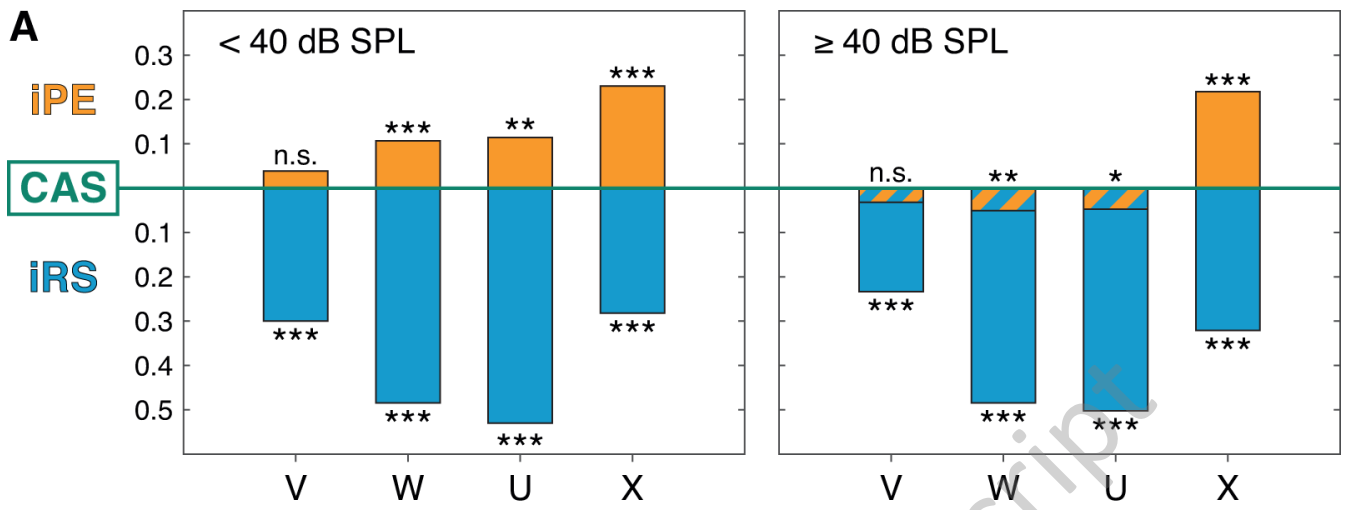
B Low intensity stimulation (< 40 dB SPL)



C High intensity stimulation (≥ 40 dB SPL)

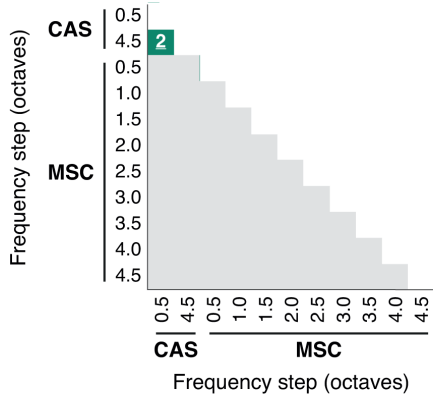


JNeurosci Accepted Manuscript



JNeurosci Accepted Manuscript

A Nonlemniscal AC: all neurons



B Nonlemniscal IC: X-neurons

